technical note technical note

Examination of Ice Accretion Predictions by 2D Computer Codes for SLD Conditions

James T. Riley
Program Manager, Aircraft Icing Research Program, William J. Hughes Technical Center, NJ 08405

Ezgi S. Oztekin
Senior Scientist, Aircraft Icing Research Program, William J. Hughes Technical Center, NJ 08405

March 2020

DOT/FAA/TC-TN19/45

U.S. Department of Transportation
Federal Aviation Administration

NOTICE

Technical Report Documentation Page

1. Report No.	2. Government Accession No.	3. Recipient's Catalog No.
DOT/FAA/TC-TN19/45		

4. Title and Subtitle	5. Report Date
Examination of Ice Accretion Predictions by 2D Computer Codes for SLD Conditions	March 2020
	6. Performing Organization Code

7. Author(s)	8. Performing Organization Report No.
James T. Riley Ezgi S. Oztekin	

9. Performing Organization Name and Address	10. Work Unit No. (TRAIS)
Federal Aviation Administration, WJH Technical Center, Atlantic City Int. Airport, NJ 08405 Diakon Solutions, LLC, 110 W Beaver Dr, Cape May Court House, NJ 08210	
	11. Contract or Grant No.

12. Sponsoring Agency Name and Address	13. Type of Report and Period Covered
Paul Pellicano FAA Southern Regional Office 1701 Columbia Ave College Park, GA 30337	
	14. Sponsoring Agency Code AIR-691

15. Supplementary Notes

The FAA William J. Hughes Technical Center Aviation Research Division COR was Timothy G. Smith.

16. Abstract

Some ice-shape comparisons can be readily done in the evaluation of 2D ice accretion computer codes for supercooled large drop (SLD) conditions. Comparisons are shown in this technical note using LEWICE2D (two-dimensional ice accretion code). Ice-shape prediction comparisons address several issues: the fidelity of icing tunnel drop distributions to Title 14 Code of Federal Regulations Part 25, Appendix O distributions; the impact of using 10-bin versus median volume diameter representations of the distributions; and the effect of liquid water content. Ice-shape predictions are also compared to experimental ice shapes from a database of SLD ice accretions developed through testing in the NASA Glenn Research Center's Ice Research Tunnel. Comparisons are conducted to investigate sensitivity to ice-shape input parameters.

17. Key Words	18. Distribution Statement
Aircraft ice accretion, Ice accretion prediction, Numerical modeling of ice growth, LEWICE2D, Aerodynamic performance degradation of ice contaminated airfoils, Aircraft icing, Icing simulation, Icing modeling, Airfoil ice, Airfoil icing	This document is available to the U.S. public through the National Technical Information Service (NTIS), Springfield, Virginia 22161. This document is also available from the Federal Aviation Administration William J. Hughes Technical Center at actlibrary.tc.faa.gov.

19. Security Classif. (of this report)	20. Security Classif. (of this page)	21. No. of Pages	22. Price
Unclassified	Unclassified	54	

TABLE OF CONTENTS

LIST OF FIGURES

LIST OF TABLES

LIST OF ACRONYMS

CFR	Code of Federal Regulations
FZDZ	Freezing drizzle
FZRA	Freezing rain
IRT	Icing research tunnel
LEWICE2D	Two-dimensional ice accretion code
LWC	Liquid water content
MVD	Median volume diameter
NACA	National Advisory Committee for Aeronautics (airfoils)
SLD	Supercooled large droplet

EXECUTIVE SUMMARY

Some ice-shape comparisons can be readily done in the evaluation of 2D ice-accretion computer codes for supercooled large drop (SLD) conditions. Comparisons are illustrated in this technical note using LEWICE2D (two-dimensional ice accretion code).

Ice-shape prediction comparisons address several issues:

- The fidelity of icing tunnel drop distributions to Title 14 Code of Federal Regulations (CFR) Part 25, Appendix O distributions
- The impact of using 10-bin versus median volume diameter representations of the distributions
- The effect of liquid water content (LWC).

Ice-shape predictions are also compared to experimental ice shapes from a database of SLD ice accretions developed through testing in the NASA Glenn Research Center's Icing Research Tunnel.

Comparisons are made to investigate sensitivity to ice-shape input parameters.

INTRODUCTION

This technical note presents comparisons that can be performed in the evaluation of the performance of 2D ice-accretion prediction computer codes for supercooled large drop (SLD) conditions. The comparisons are shown using versions of two-dimensional ice accretion code developed at NASA Lewis LEWICE 2D obtained from NASA [1]. The versions used are recent (dating back no more than 2 years), but may have been superseded by later versions differing in some respects.

The ice-shape prediction comparisons fall into several categories:

- Title 14 CFR Part 25, Appendix O distributions versus NASA Glenn Icing Research Tunnel (IRT) SLD distributions for a case with LWC = 0.82 g/m^3
- 14 CFR 25, Appendix O distributions using 10-bin representations versus median volume diameter (MVD) representations for the same case with LWC = 0.82 g/m^3
- 14 CFR 25, Appendix O distributions using 10-bin representations versus MVD representations for the same case, except LWC is determined from Appendix O LWC curves
- SLD conditions using MVD representations versus experimental ice shapes from a database of SLD ice accretions developed through testing in NASA's IRT
- Sensitivity to ice shape input parameters

The comparisons suggest that 2D ice-accretion computer codes may not be highly sensitive to differences in SLD drop distributions with 10-bin distributions.

ICE SHAPE PREDICTION COMPARISONS

COMPARISON OF ICE-SHAPE PREDICTIONS FOR APPENDIX O AND IRT DROP SIZE DISTRIBUTIONS USING 10-BIN REPRESENTATIONS

Appendix O of 14 CFR 25, provided in appendix A of this document, includes four drop size distributions for certification for SLD conditions:

- Freezing drizzle (FZDZ) environments, MVD $\leq$ 40 μm
- FZDZ, MVD > 40 μm
- Freezing rain (FZRA) environments, MVD $\leq$ 40 μm
- FZRA, MVD > 40 μm

These distributions can be simulated to varying degrees of accuracy in the IRT [2].

The Appendix O and IRT distributions can be represented using the midpoints of 10 bins, as shown in tables 1–4. In tables 1 and 2, the numbers in parentheses in the IRT 2014 columns are the spraybar air and delta (water minus air) pressure settings that created the condition.

Table 1. 10-bin drop diameter representation for IRT and Appendix O, FZDZ, MVD ≤ 40 μm

Bin	Cum Mass	Upper Cum. Mass Bound.	Fraction of LWC	IRT 2014 (15,10) midpoint	IRT 2014 (15,20) midpoint	FZDZ, MVD ≤ 40 μm midpoint
1	0.05	0.1	0.1	8.2	9	8.5
2	0.2	0.3	0.2	11.6	15	12.5
3	0.4	0.5	0.2	16.5	29	17.5
4	0.6	0.7	0.2	23	51	22.8
5	0.75	0.8	0.1	30.6	77	28.8
6	0.825	0.85	0.05	36.5	105	34.5
7	0.875	0.9	0.05	41	129	45.5
8	0.925	0.95	0.05	51	165	95.5
9	0.9625	0.975	0.025	65	195	165.5
10	0.9875	1	0.025	96	240	254

Table 2. 10-bin drop diameter representation for IRT and Appendix O, FZDZ, MVD > 40 μm

Bin	Cum Mass	Upper Cum. Mass Bound.	Fraction of LWC	IRT 2014 (4,25) midpoint	IRT 2014 (6,50) midpoint	FZDZ, MVD > 40 μm midpoint
1	0.05	0.1	0.1	17.5	15.5	10.5
2	0.2	0.3	0.2	45.5	49	21.5
3	0.4	0.5	0.2	92	106	66
4	0.6	0.7	0.2	153	173	155
5	0.75	0.8	0.1	202.3	242	226
6	0.825	0.85	0.05	240	290	265.5
7	0.875	0.9	0.05	270	330	295.5
8	0.925	0.95	0.05	325	380	333
9	0.9625	0.975	0.025	380	445	372.5
10	0.9875	1	0.025	460	540	418.5

Table 3. 10-bin drop diameter representation for IRT and Appendix O, FZRA, MVD ≤ 40 μm

Bin	Cum Mass	Upper Cum. Mass Bound.	Fraction of LWC	IRT 2015, MVD=270μm midpoint	FZRA, MVD ≤ 40 μm midpoint
1	0.05	0.1	0.1	44.5	6.4
2	0.2	0.3	0.2	127	9.5
3	0.4	0.5	0.2	218	14.5
4	0.6	0.7	0.2	325	24.5
5	0.75	0.8	0.1	440	259
6	0.825	0.85	0.05	500	535
7	0.875	0.9	0.05	565	655
8	0.925	0.95	0.05	630	792
9	0.9625	0.975	0.025	750	942
10	0.9875	1	0.025	920	1191

Table 4. 10-bin drop diameter representation for IRT and Appendix O, FZRA, MVD > 40 μm

Bin	Cum Mass	Upper Cum. Mass Bound.	Fraction of LWC	IRT 2015, MVD=270μm midpoint	FZRA, MVD >40 μm midpoint
1	0.05	0.1	0.1	44.5	8.8
2	0.2	0.3	0.2	127	36
3	0.4	0.5	0.2	218	400
4	0.6	0.7	0.2	325	645
5	0.75	0.8	0.1	440	833
6	0.825	0.85	0.05	500	956
7	0.875	0.9	0.05	565	1066
8	0.925	0.95	0.05	630	1196
9	0.9625	0.975	0.025	750	1346
10	0.9875	1	0.025	920	1546

Comparison of ice shapes predicted using 10-bin representations for the IRT distributions and Appendix O distribution provide an indication of how sensitive the ice-accretion prediction code is to the differences between the Appendix O and IRT distributions. This is shown in figures 1–8, using two-dimensional ice accretion code (LEWICE2D) for a National Advisory Committee for Aeronautics (NACA) 4415(mod) airfoil.

The following are the input conditions:

c = 1.9812 m,

$\alpha = 0°$,

U_∞ = 87.2 m/s,

LWC = 0.82 g/m^3,

T_∞ = 266.85 K,

P_∞ = 100,000 pascal,

RH = 100%,

t = 20 minutes

where c is chord length, α is angle of attack, U_∞, T_∞ and P_∞ are freestream velocity, temperature and pressure, respectively, RH is relative humidity, and t is duration.

FZDZ, MVD ≤ 40 µm

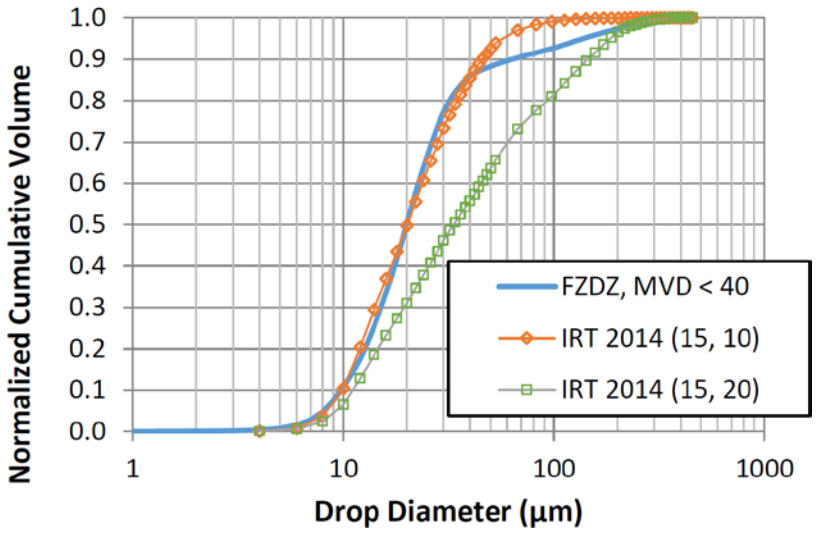

Figure 1. Drop distributions for Appendix O, FZDZ, MVD ≤ 40 µm (figure 13a of Ref [2])

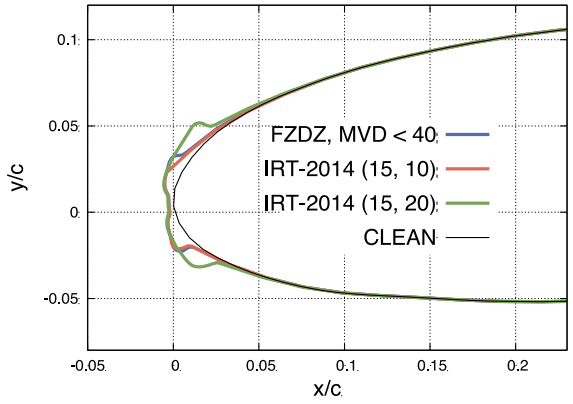

Figure 2. Ice-accretion predictions for 10-bin drop diameter representations

FZDZ, MVD > 40 µm

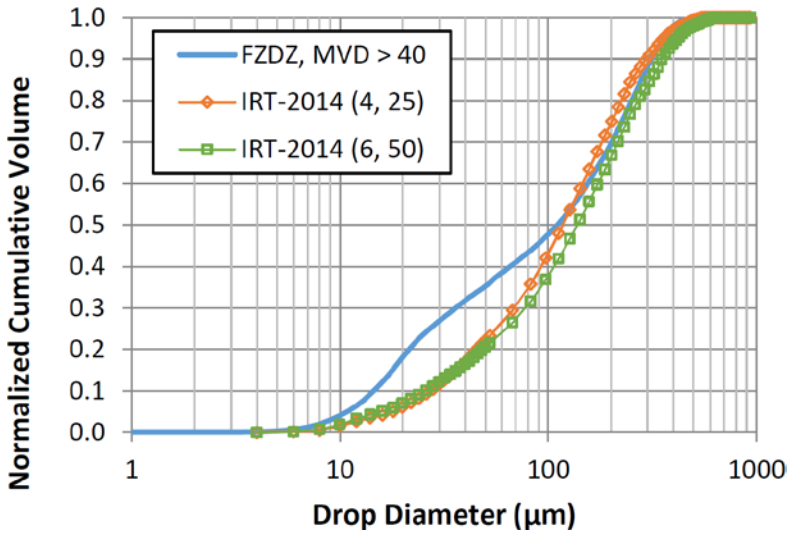

Figure 3. Drop distributions for Appendix O, FZDZ, MVD > 40 µm (figure 13b of Ref [2])

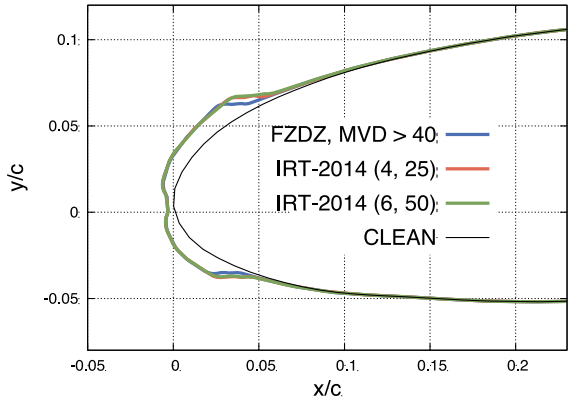

Figure 4. Ice-accretion predictions for 10-bin drop diameter representations

FZRA, MVD ≤ 40 µm

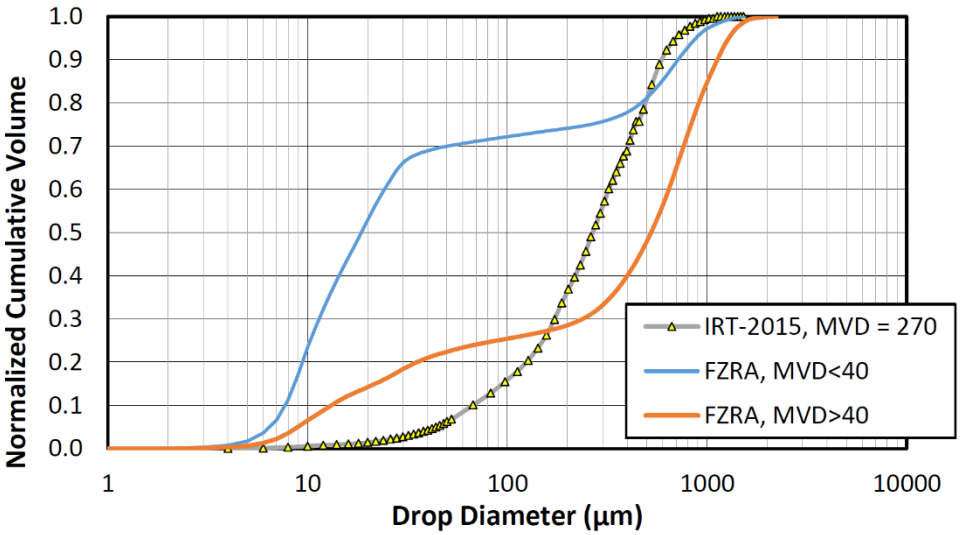

Figure 5. Drop distributions for Appendix O, FZRA, MVD ≤ 40 µm (figure 13c of Ref [2])

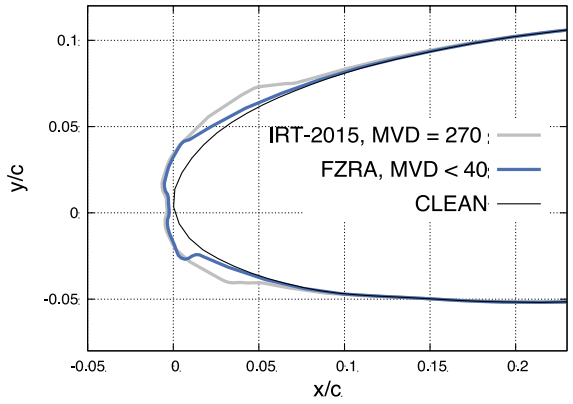

Figure 6. Ice-accretion predictions for 10-bin drop diameter representations

FZRA, MVD > 40 µm

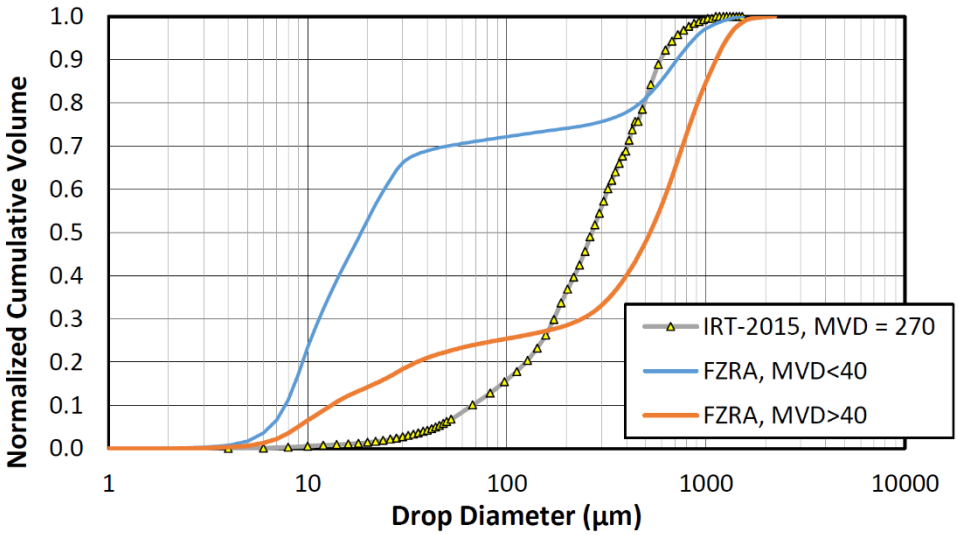

Figure 7. Drop distributions for Appendix O, FZRA, MVD > 40 µm (figure 13c of Ref [2])

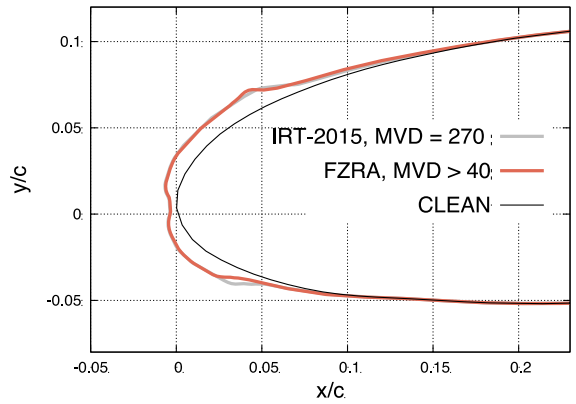

Figure 8. Ice-accretion predictions for 10-bin drop diameter representations

<u>COMPARISON OF ICE-SHAPE PREDICTIONS FOR APPENDIX O DROP SIZE DISTRIBUTIONS USING 10-BIN AND MVD REPRESENTATIONS, LWC = 0.82 G/M^3</u>

The four Appendix O SLD distributions can be represented using the midpoints of 10 bins, as shown in section 1, tables 1–4, and also by using the MVD of the distribution.

The MVDs are:

- FZDZ, MVD ≤ 40 µm: MVD = 20 µm
- FZDZ, MVD > 40 µm: MVD = 110 µm
- FZRA, MVD ≤ 40 µm: MVD = 19 µm

- FZRA, MVD > 40 μm: MVD = 526 μm

Comparison of ice shapes predicted using the 10-bin representation and the MVD representation of the Appendix O distribution provides an indication of how sensitive the ice-accretion prediction code is to the differences between these two representations. This is shown in figures 9–16 using LEWICE2D for a NACA4415(mod) airfoil.

The input conditions are the same as those used in section 1, as follows:

c = 1.9812 m,

$\alpha = 0°$,

U_∞ = 87.2 m/s,

LWC = 0.82 g/m^3,

T_∞ = 266.85 K,

P_∞ = 100,000 pascal,

RH = 100%,

t = 20 minutes

where c is chord length, α is angle of attack, U_∞, T_∞ and P_∞ are freestream velocity, temperature and pressure, respectively, RH is relative humidity, and t is duration.

Note that the conditions include an LWC of 0.82 g/m^3, substantially larger than the LWCs possible for any of the four environments in Appendix O.

Models using the Appendix O distribution or just the MVD of the distribution yield very similar ice shapes that have only slight differences near the impingement limits, except for the FZRA, MVD $\leq$ 40 μm conditions (see figures 9, 11, and 15). Predictions for this case are more sensitive to the representation of the droplet distribution.

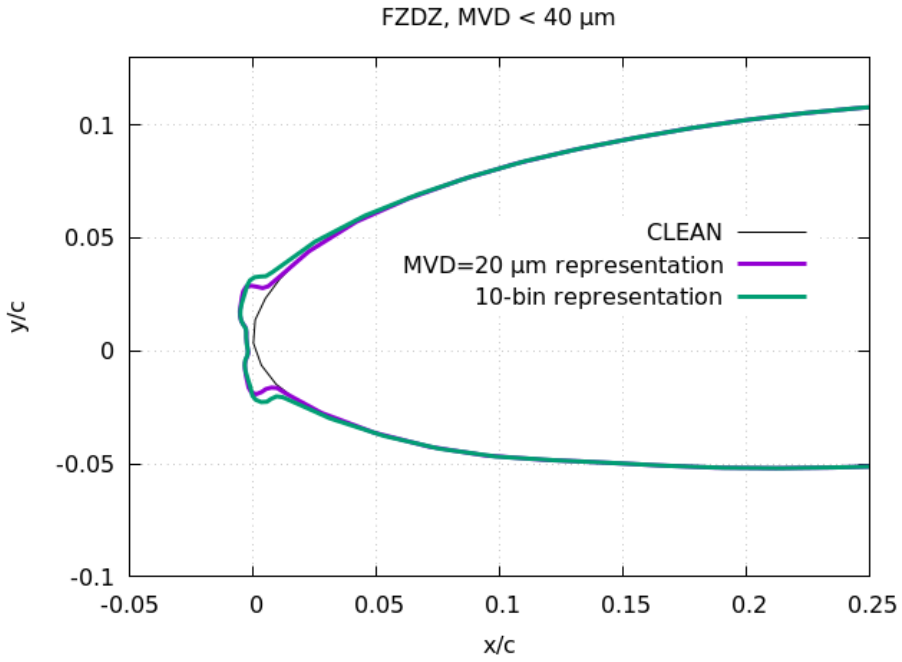

Figure 9. Ice accretions for 10-bin and MVD representations of Appendix O, FZDZ, MVD ≤ 40µm distribution

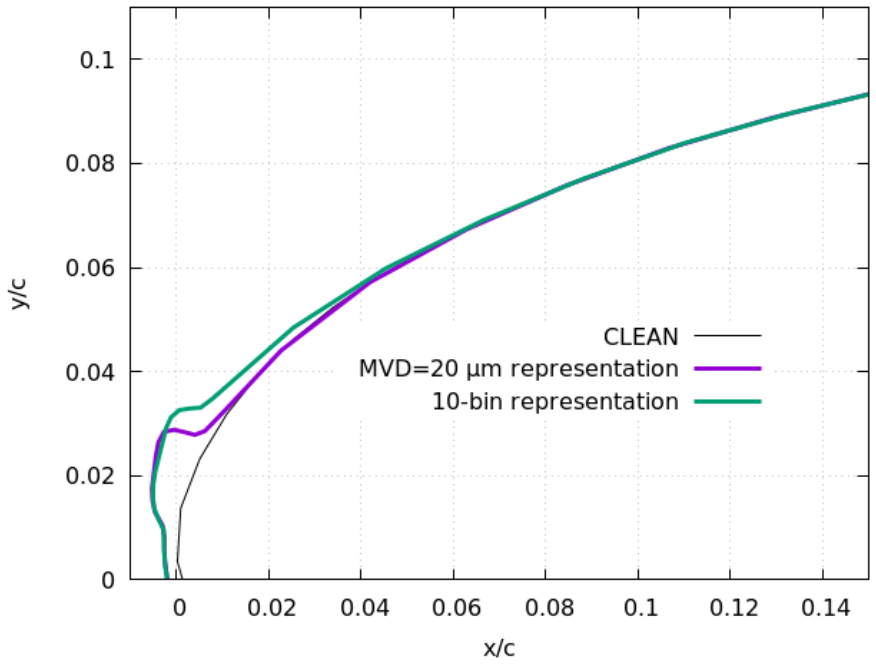

Figure 10. Close-up view of upper surface

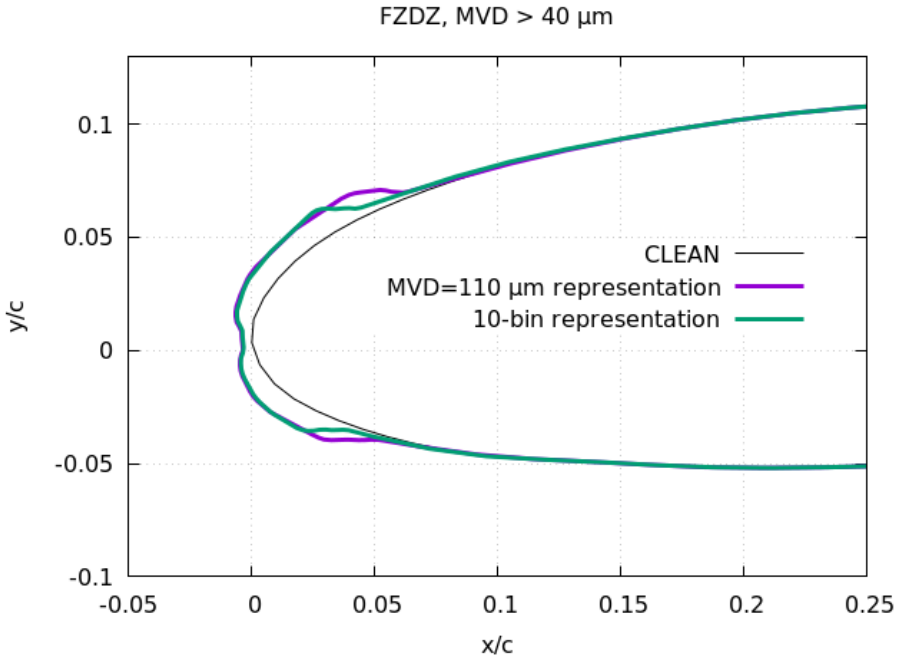

Figure 11. Ice accretions for 10-bin and MVD representations of Appendix O, FZDZ, MVD > 40µm distribution

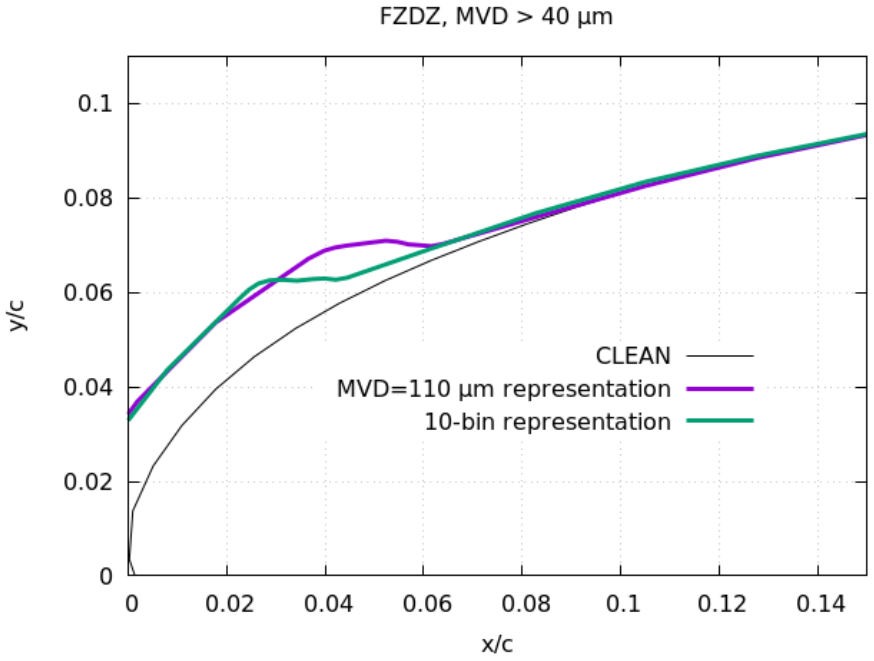

Figure 12. Close-up view of upper surface

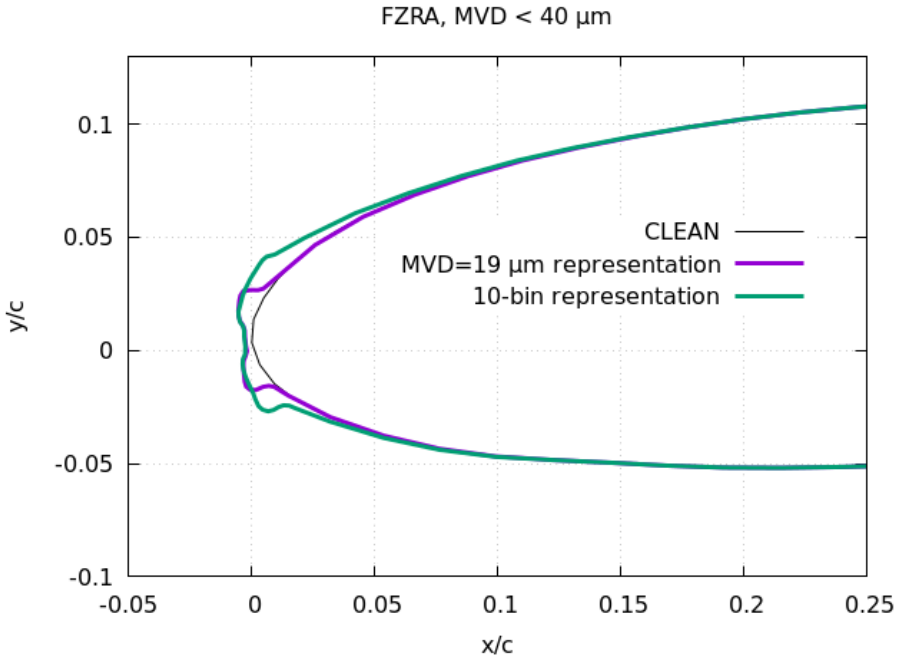

Figure 13. Ice accretions for 10-bin and MVD representations of Appendix O, FZRA, MVD ≤ 40µm distribution

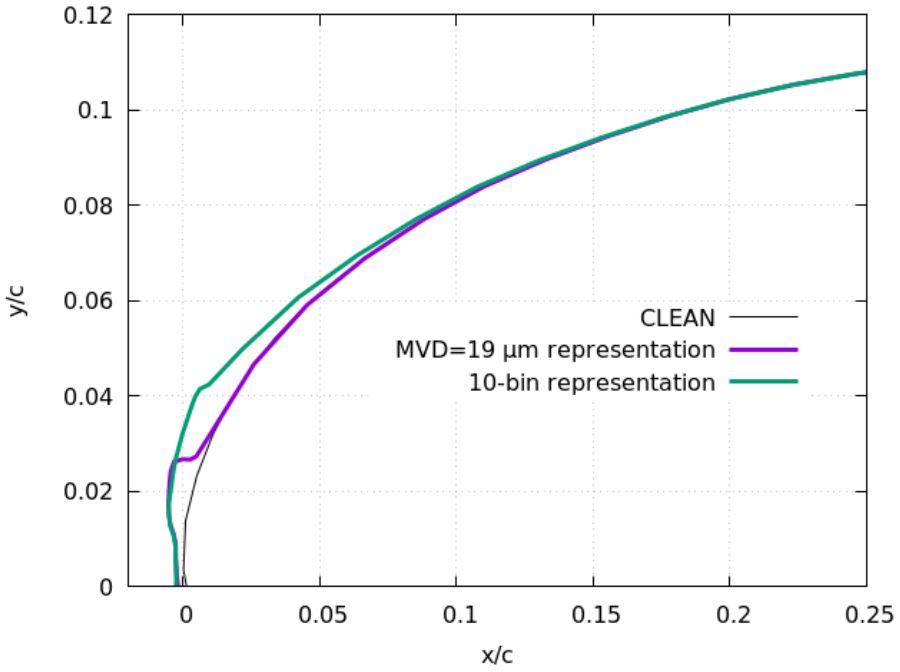

Figure 14. Close-up view of upper surface

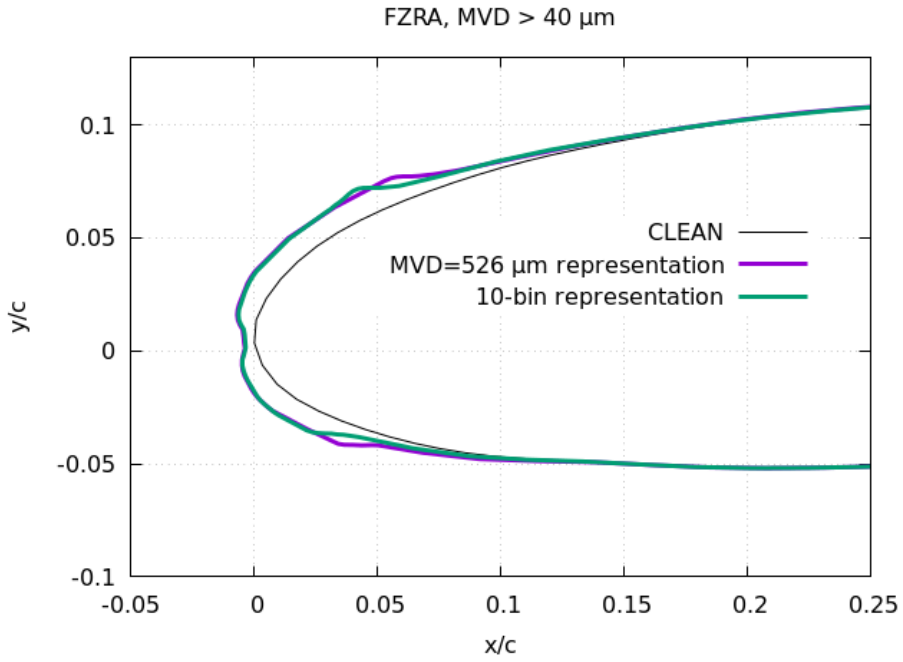

Figure 15. Ice accretions for 10-bin and MVD representations of Appendix O, FZRA, MVD > 40µm distribution

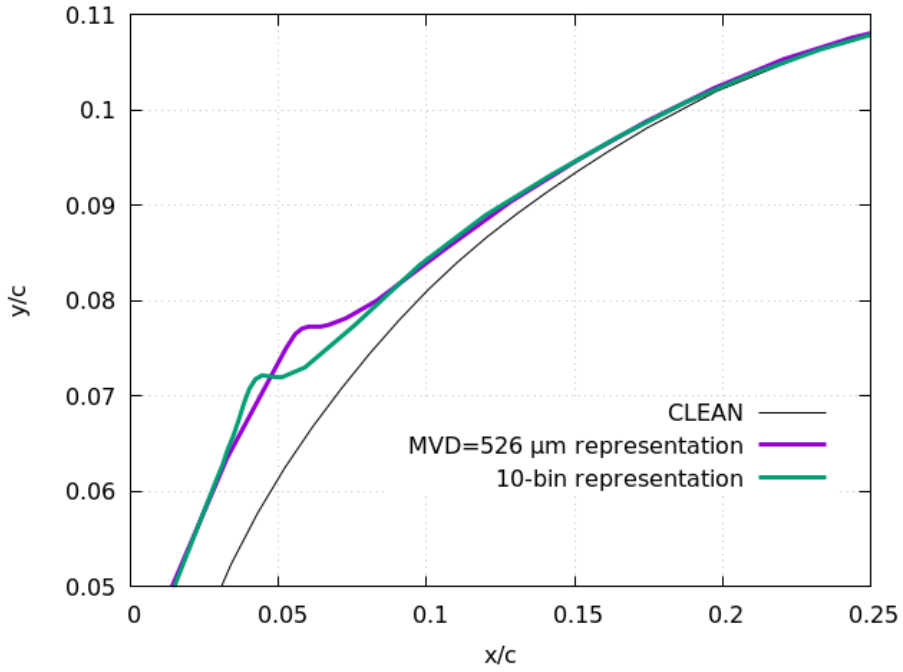

Figure 16. Close-up view of upper surface

COMPARISON OF ICE-SHAPE PREDICTIONS FOR APPENDIX O DROP SIZE DISTRIBUTIONS USING 10-BIN AND MVD REPRESENTATIONS, LWC DETERMINED FROM APPENDIX O CURVES

The four Appendix O SLD distributions can be represented using the midpoints of 10 bins, as shown in section 1 (see tables 1–4), and also by using just the MVD of the distribution as shown in section 2 and tabulated in table 5. The LWC of 0.82 g/m^3 employed in the previous two sections are substantially larger than the LWCs possible for any of the four environments in Appendix O calculated in this section.

To determine LWC, first use figure 1 in Appendix O. For the temperature of -6.3°C (266.85 K), this gives an approximate LWC of 0.40 g/m^3. However, for a velocity of 87.2 m/s and a duration of 20 minutes, the horizontal extent is 56.5 nautical miles. According to figure 7 in Appendix O, this gives an LWC scale factor of approximately 0.9. Using this scale factor, an LWC of approximately 0.36 g/m^3 was calculated. Following the same procedure, LWC for FZDZ, MVD>40μm; FZRA, MVD≤40μm; and FZRA, MVD>40μm are 0.22, 0.25, and 0.21 g/m^3, respectively. Table 5 summarizes the LWC values calculated for the four Appendix O SLD distributions.

Table 5. Calculated values of LWC in Appendix O conditions

	MVD (μm)	LWC (g/m^3)
FZDZ, MVD ≤ 40	20	0.36
FZDZ, MVD > 40	110	0.22
FZRA, MVD ≤ 40	19	0.25
FZRA, MVD > 40	526	0.21

Comparison of ice shapes predicted using the 10-bin representation and the MVD representation of the Appendix O distribution provide an indication of how sensitive the ice-accretion prediction code is to the differences between these two representations at the LWC levels determined from Appendix O curves. This is shown in figures 17–24 using LEWICE2D for a NACA4415(mod) airfoil.

The input conditions are the same as those used in section 1, except for the LWC, as follows:

c = 1.9812 m,

$\alpha = 0°$,

U_∞ = 87.2 m/s,

LWC = determined from Appendix O curves (g/m^3) (see table 5),

T_∞ = 266.85 K,

P_∞ = 100,000 pascal,

RH = 100%,

t = 20 minutes

where c is chord length, α is angle of attack, U_∞, T_∞ and P_∞ are freestream velocity, temperature and pressure, respectively, RH is relative humidity, and t is duration.

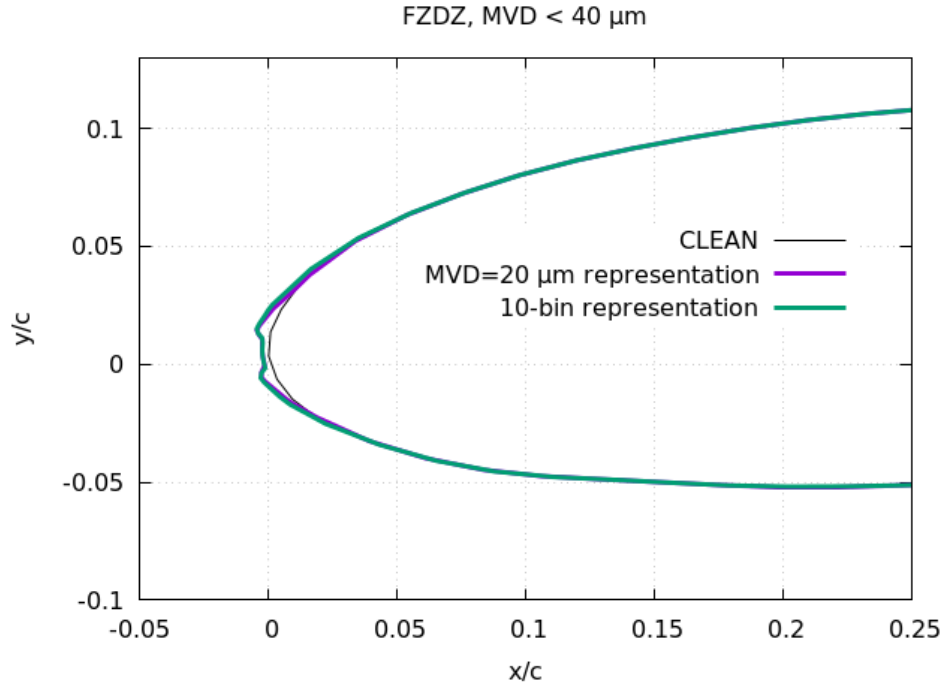

Figure 17. Ice accretions for 10-bin and MVD representations of Appendix O, FZDZ, MVD ≤ 40µm distribution, LWC = 0.36 g/m^3

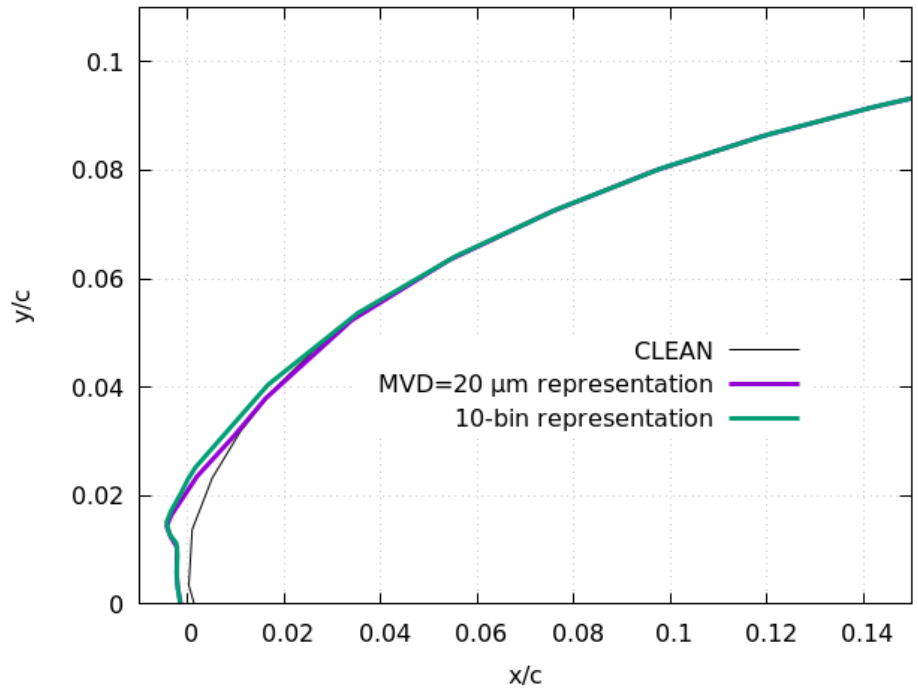

Figure 18. Close-up view of upper surface

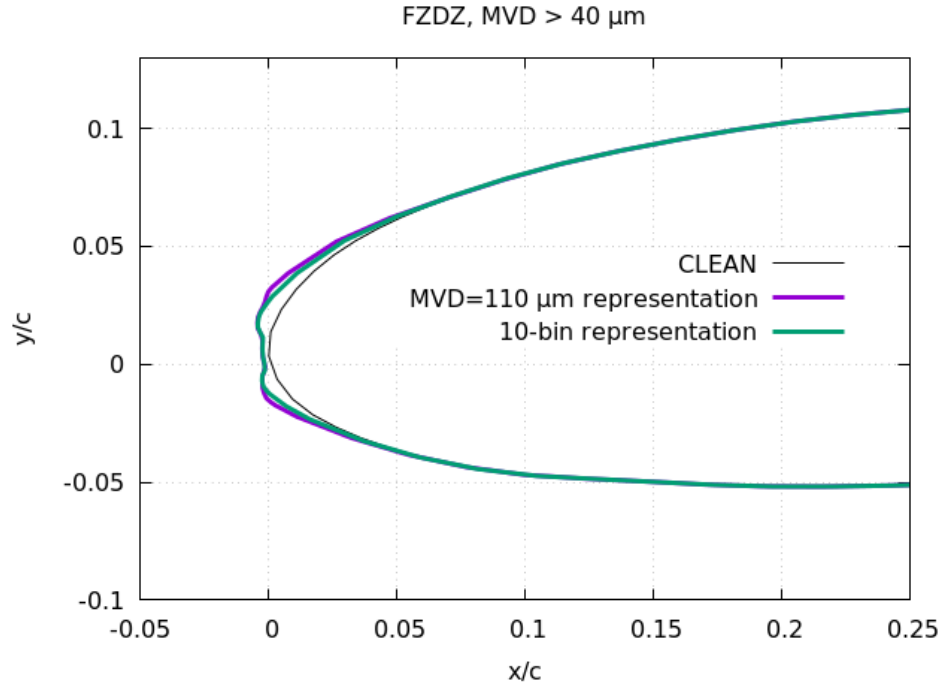

Figure 19. Ice accretions for 10-bin and MVD representations of Appendix O, FZDZ, MVD > 40µm distribution, LWC = 0.22 g/m^3

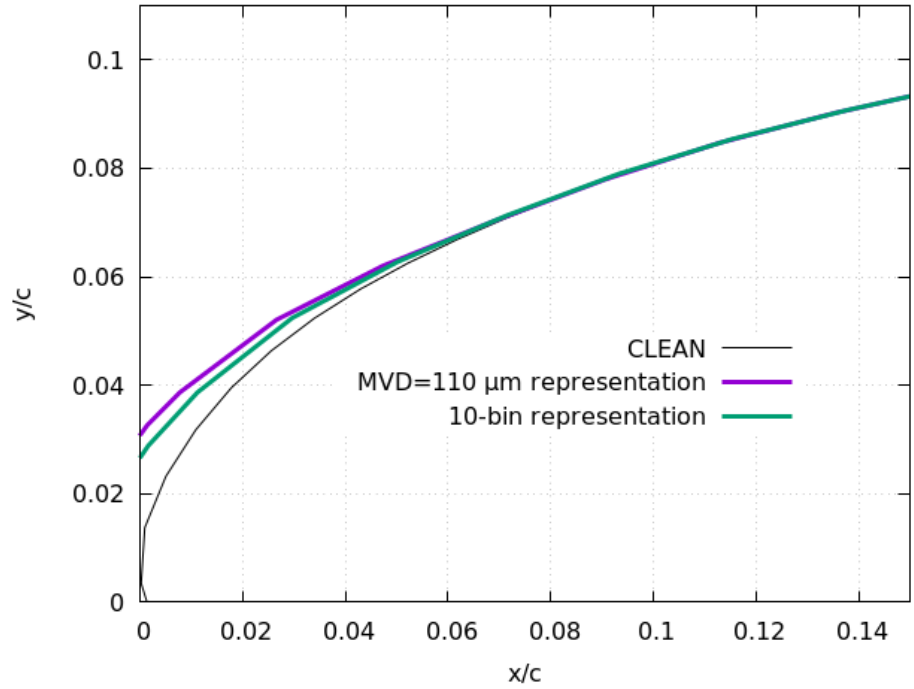

Figure 20. Close-up view of upper surface

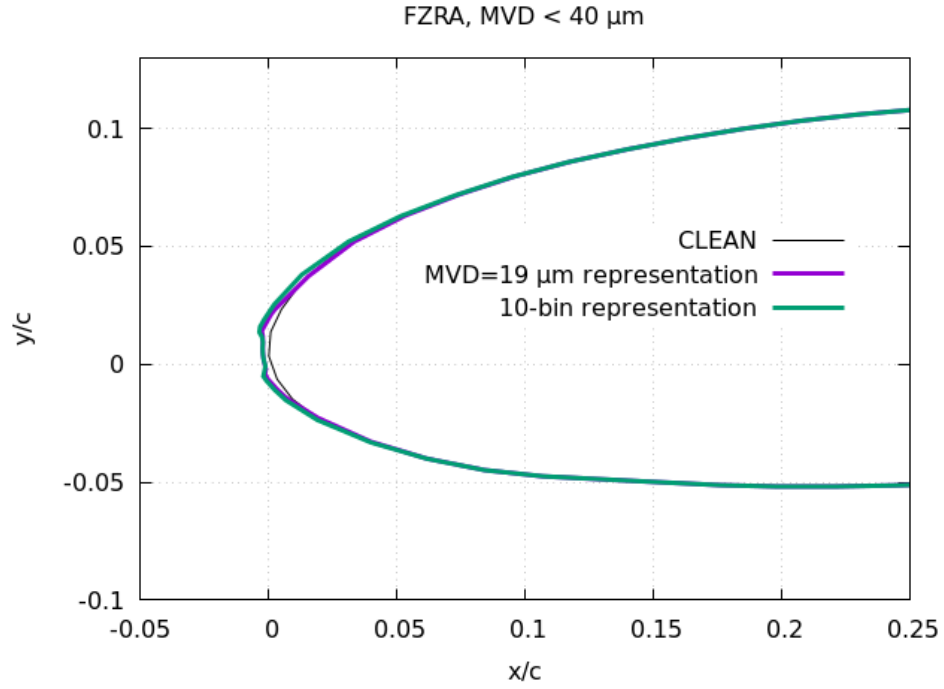

Figure 21. Ice accretions for 10-bin and MVD representations of Appendix O, FZRA, MVD ≤ 40µm distribution, LWC = 0.25 g/m^3

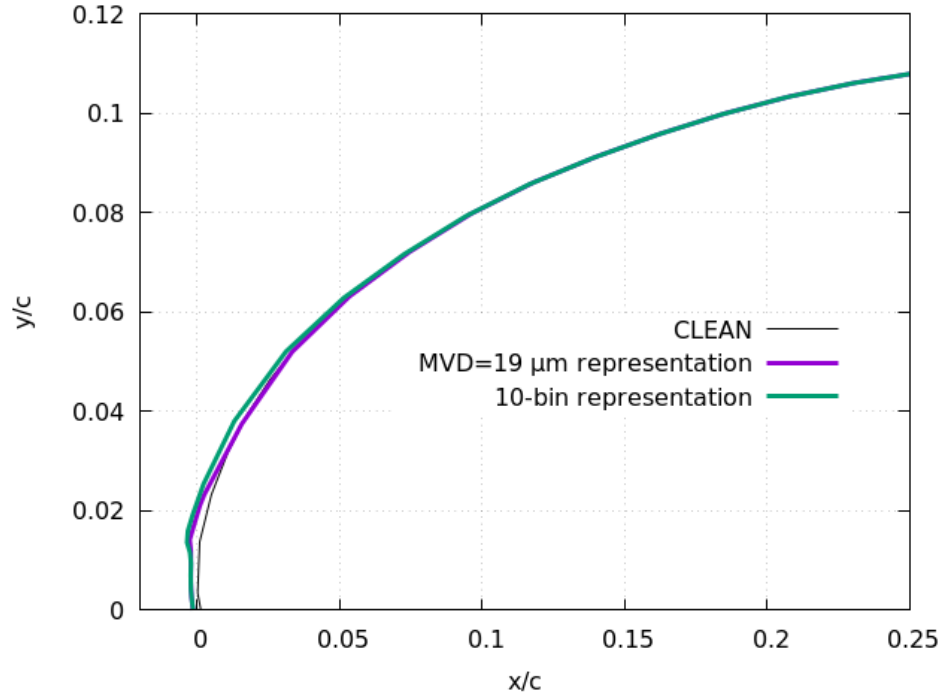

Figure 22. Close-up view of upper surface

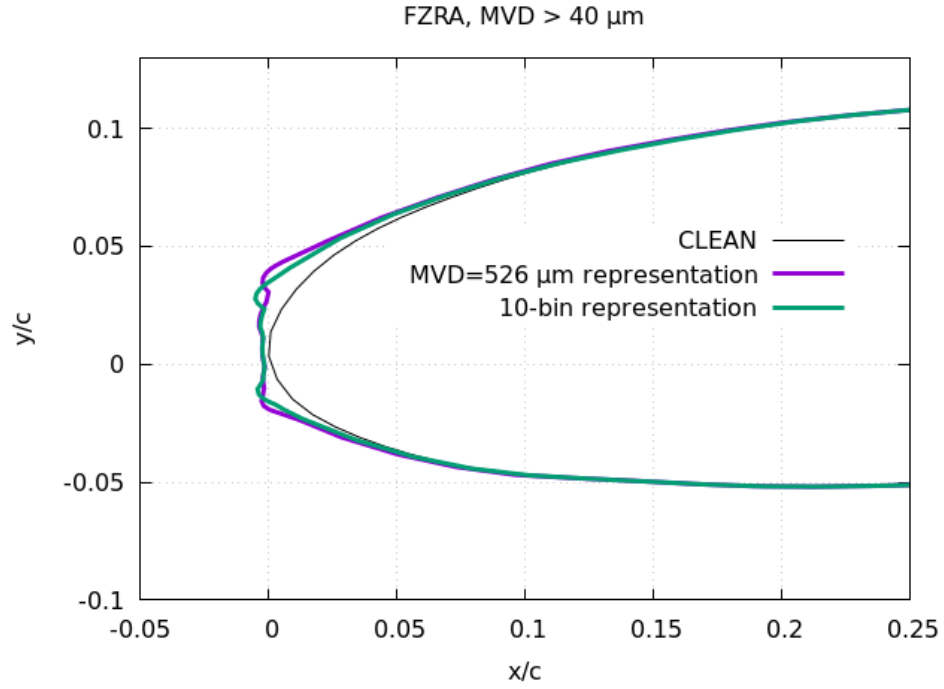

Figure 23. Ice accretions for 10-bin and MVD representations of Appendix O, FZRA, MVD > 40µm distribution, LWC = 0.21 g/m^3

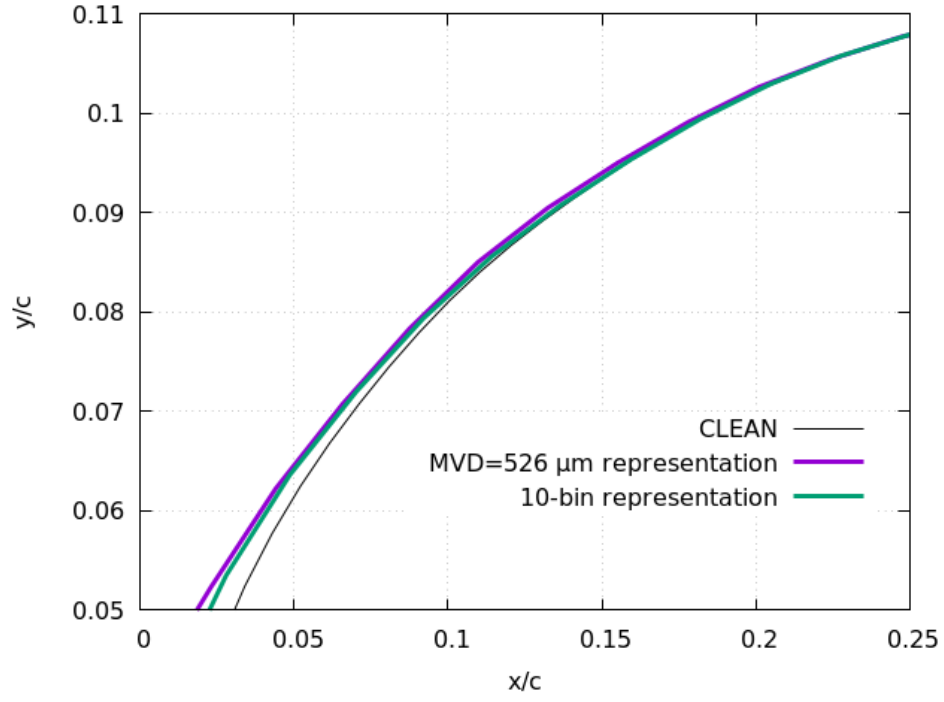

Figure 24. Close-up view of upper surface

COMPARISON OF ICE-SHAPE PREDICTIONS FOR APPENDIX O DROP SIZE DISTRIBUTIONS AND EXPERIMENTAL DATA USING MVD REPRESENTATIONS

A database of experimental ice accretions for SLD ice accretions was developed through testing in NASA's IRT [3]. Identical cloud and flight conditions were generated for five different airfoil models. The models chosen represent a variety of aircraft types from the horizontal stabilizer of a large transport aircraft to the wings of regional, business, and general aviation aircraft (see table 6 and figure 25). In addition to the standard documentation methods of 2D ice shape tracing and imagery, ice-mass measurements were also taken. This database is a valuable resource for the evaluation of the performance of ice-accretion prediction codes under SLD conditions. The database is available from NASA's Glenn Research Center on request. It is documented in reference [3].

Table 6. Airfoil models and geometric parameters

	Chord, c (in)	Maximum thickness, t (in)	Dimensionless thickness, t/c (%)	Leading edge radius, r_{LE}/c (%)
NLF 0414	36	5.1	14.2	2.2 [2.4][1]
NACA 23012	72	8.6	12	2.6 [2.9]
GLC 305	36	3.2	9	1.6
Commercial tail	36	3.2	9	1.8
Business jet wing	61	8.5	14	3.2

Use of the database is shown with LEWICE2D for a selection of cases (see table 7). For each model, comparisons at MVD = 40 and MVD = 225 μm are made at two speeds, U_∞ =100 and U_∞ = 250 knots, corresponding to the total temperatures of T_t = -5°C and T_t = -10°C, respectively (see figures 26–30). The spray time was held constant at 10 minutes. The angle of attack is 2 degrees for all, except for the business jet wing for which it is 3 degrees.

[1] Values in square brackets are taken from the following website http://www.airfoildb.com/airfoils, retrieved in 2018

Table 7. Airfoil models, test conditions, and measured ice mass

	MVD (μm)	U_∞ (knots)	T_∞ (^oC)	LWC (g/m^3)	Ice mass (g)	Test No
NLF 0414	40	100	-5	0.32	252	IF1281
	36	250	-10	0.24	479	IF1317
	225	100	-5	1.39	1087	IF1287
	225	250	-10	0.37	1265	IF1322
NACA 23012	40	100	-5	0.32	345	EG1324
	36	250	-10	0.24	642	EG1358
	225	100	-5	1.39	1394	EG1331
	225	250	-10	0.38	2129	EG1364
GLC 305	40	100	-5	0.32	155	TF1515
	36	250	-10	0.24	298	TF1514
	225	100	-5	1.39	632	TF1516
	225	250	-10	0.38	787	TF1505
Commercial tail	40	100	-5	0.32	186	JF1539
	36	250	-10	0.24	NA	JF1576
	225	100	-5	1.39	729	JF1545
	225	250	-10	0.38	NA	JF1579
Business jet wing	40	100	-5	0.32	340	NG1588
	46	200	-10	0.23	617	NG1618
	225	100	-5	1.39	1280	NG1597
	225	200	-10	0.80	2031	NG1624

Comparing figures 26a–30a, note that the experimental data show the expected trend for model chord size. For example, when scaled to chord size, more ice accretes for figure 26a for a chord of 36 inches than for figure 27a for a chord of 72 inches. The ice predictions also follow the expected trend.

The experimental and predicted ice also generally follow the expected trend for figures 26b–30b, figures 26c–30c, and figures 26d–30d.

Figures 26a and 26b have an MVD of 40 μm, and figures 26c and 26d have an MVD of approximately 225 μm. In general, the experimental ice shapes are more irregular with larger protuberance and feathers for MVD = 225 μm than for MVD = 40 μm.

This is shown by direct comparison between figure 26b (MVD = 40 μm) and figure 26d (MVD = 225 μm), as they have the same U, T_t, and LWCs, differing only by 0.13 g/m^3. The ice shape in figure 26d is substantially larger than that in figure 26b, more than can be attributed to the difference in LWC. Note that the ice shape in figure 26d is more irregular with larger protuberances

and feathers than that in figure 26b. The ice-shape predictions for figure 26d are larger than for 26b but do not reflect irregularity of the shapes.

Similar observations can be made for figures 27–29 but not for figure 30 because of the much larger difference in LWC.

Comparisons of figures 26a (40 μm) and 26c (225 μm) are difficult to interpret because there is a large difference in LWC. This also applies for figures 27–30.

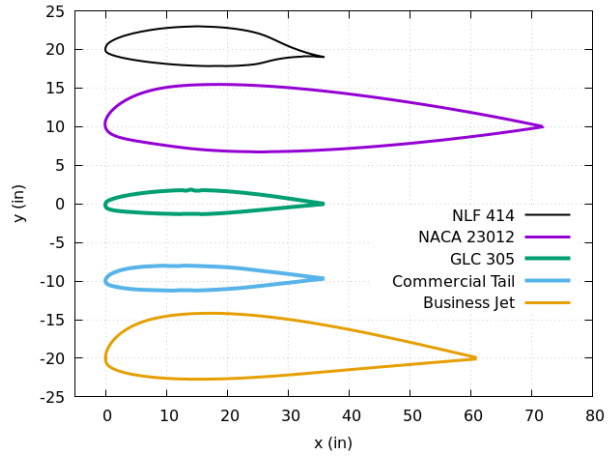

(a) Dimensional models (in inches)

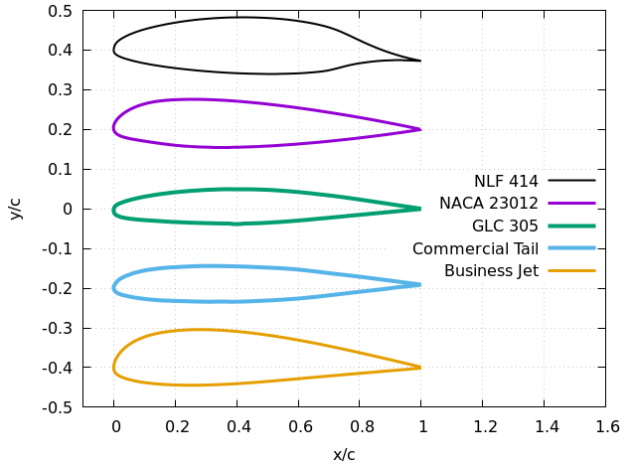

(b) Nondimensionalized models

Figure 25. Models used in SLD database of ice accretions: (a) dimensions in inches, (b) nondimensionalized by chord "c"

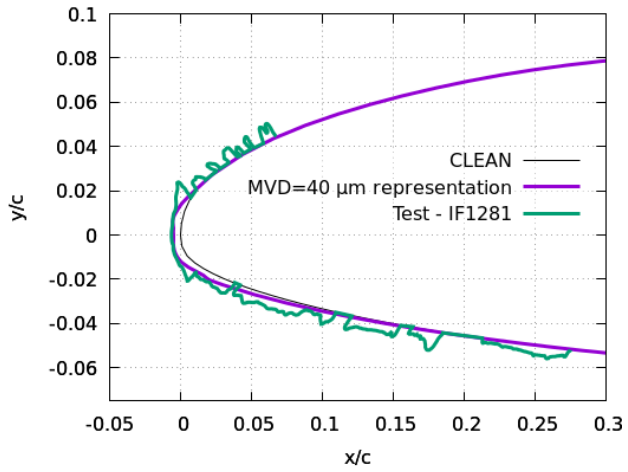

(a) MVD=40µm, U_∞=100kts, T_t=-5°C, LWC=0.32g/m^3

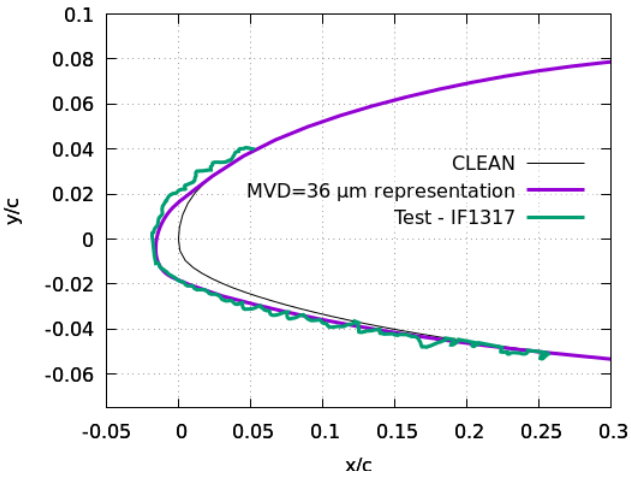

(b) MVD=36µm,U_∞=250kts, T_t=-10°C, LWC=0.24 g/m^3

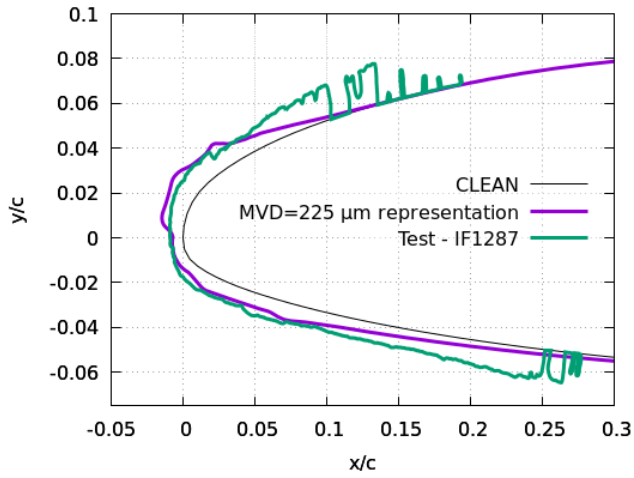

(c) MVD=225 µm, U_∞=100kts, T_t=-5°C, LWC=1.39 g/m^3

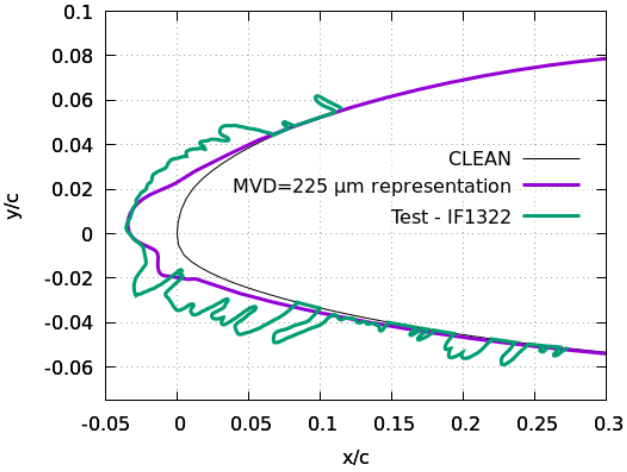

(d) MVD=225 µm, U_∞=250kts, T_t=-10°C, LWC=0.37 g/m^3

Figure 26. NLF 0414 (chord = 36 inches): (a) (b) MVD ≈ 40 µm; (c) (d) MVD = 225 µm; (a) (c) U_∞ = 100 kts, T_t = -5°C; (b) (d) U_∞ = 250 kts, T_t = -10°C

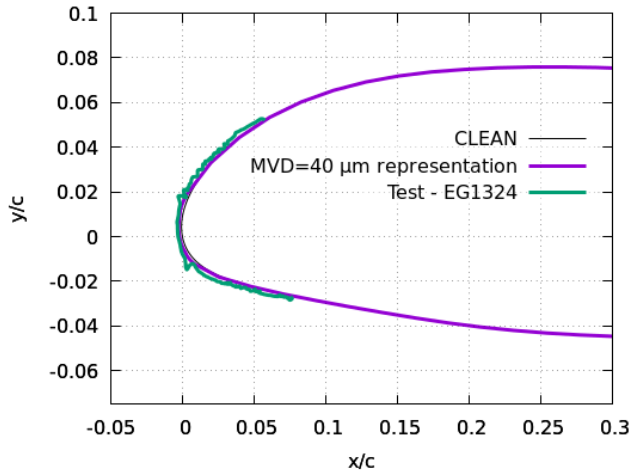

(a) MVD=40µm, U_∞=100kts, T_t=-5°C, LWC=0.32 g/m^3

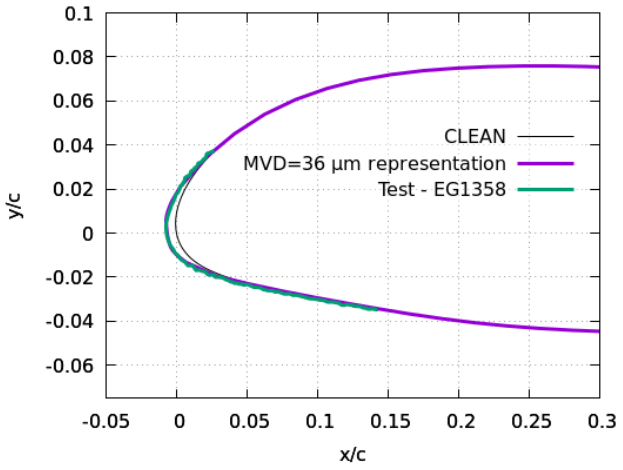

(b) MVD=36 µm, U_∞=250kts, T_t=-10°C, LWC=0.24 g/m^3

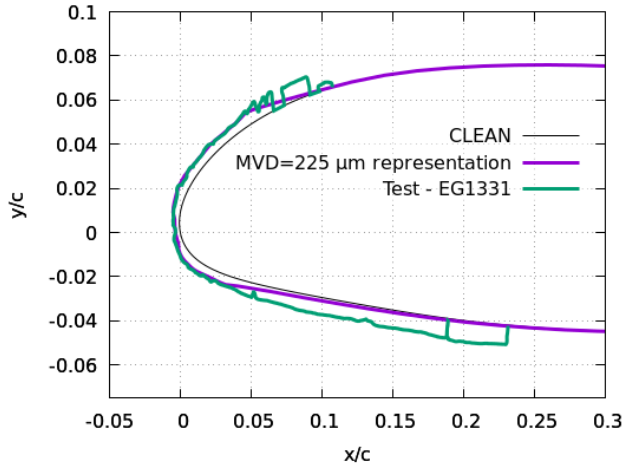

(c) MVD=225µm, U_∞=100kts, T_t=-5 °C, LWC=1.39 g/m^3

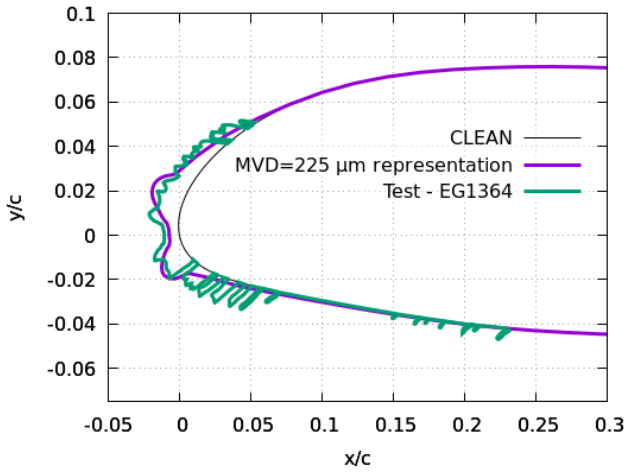

(d) MVD=225µm, U_∞=250kts, T_t=-10°C, LWC=0.38 g/m^3

Figure 27. NACA 23012 (chord = 72 inches): (a) (b) MVD ≈ 40 µm; (c) (d) MVD = 225 µm; (a) (c) U_∞ = 100 kts, T_t = -5°C; (b)(d) U_∞ = 250 kts, T_t = -10°C

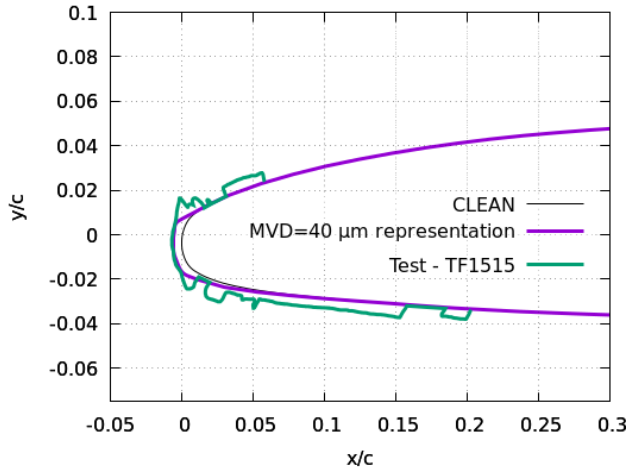

(a) MVD=40µm, U_∞=100kts, T_t=-5°C, LWC=0.32 g/m^3

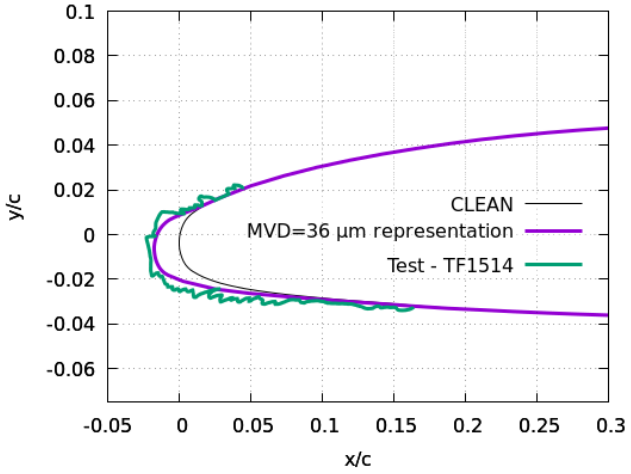

(b) MVD=36 µm, U_∞=250kts, T_t=-10°C, LWC=0.24 g/m^3

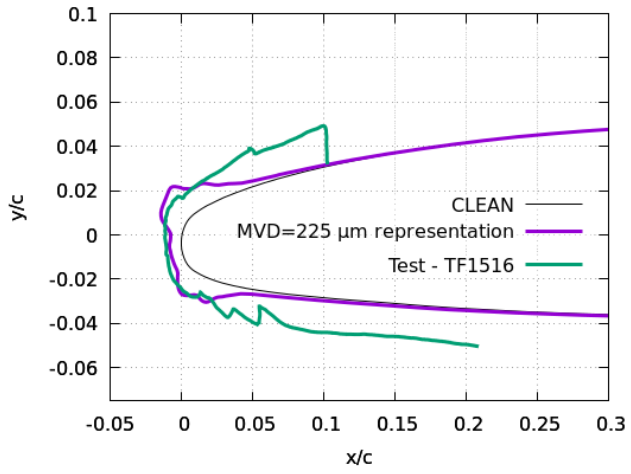

(c) MVD=225µm, U_∞=100kts, T_t=-5 °C, LWC=1.39g/m^3

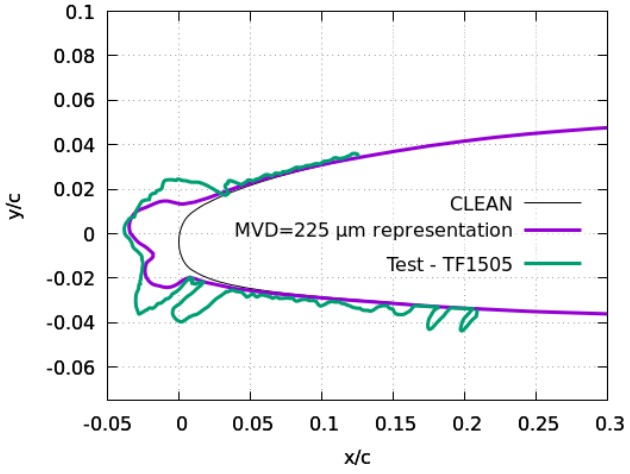

(d) MVD=225 µm, U_∞=250kts, T_t=-10°C, LWC=0.38g/m^3

Figure 28. GLC 305 (chord = 36 inches): (a) (b) MVD ≈ 40 µm; (c) (d) MVD = 225 µm; (a) (c) U_∞ = 100 kts, T_t=-5°C; (b) (d) U_∞ = 250 kts, T_t = -10°C

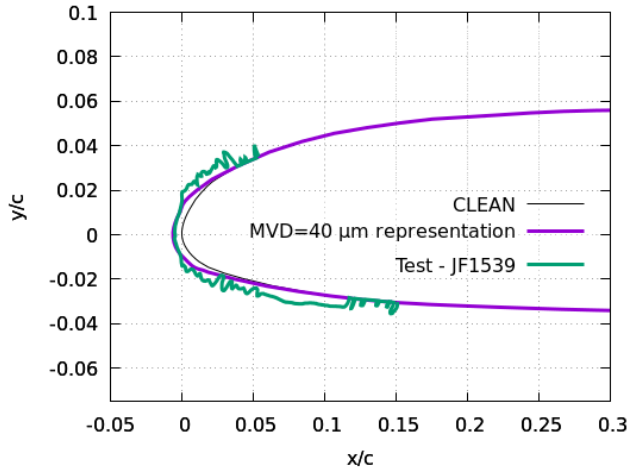

(a) MVD=40µm, U_∞=100 kts, T_t=-5°C, LWC=0.32 g/m^3

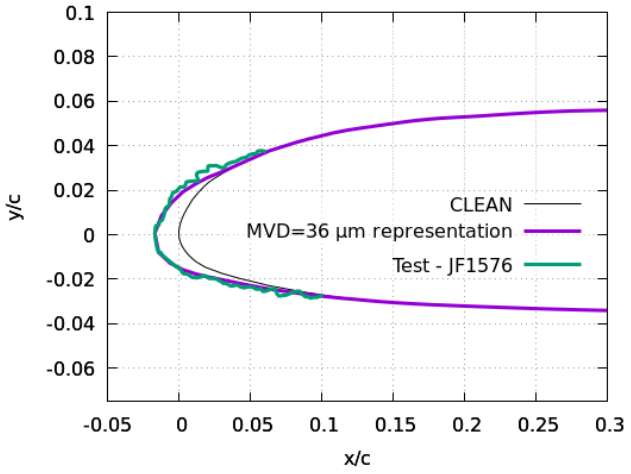

(b) MVD=36µm, U_∞ = 250 kts, T_t = -5 °C, LWC=0.24 g/m^3

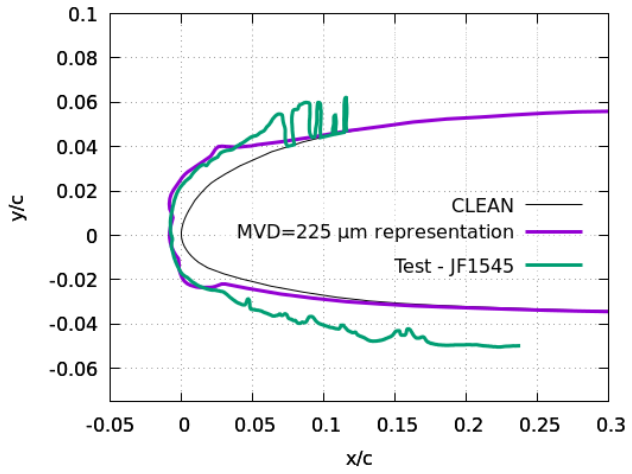

(c) MVD =225µm, U_∞=100kts, T_t=-5°C, LWC=1.39 g/m^3

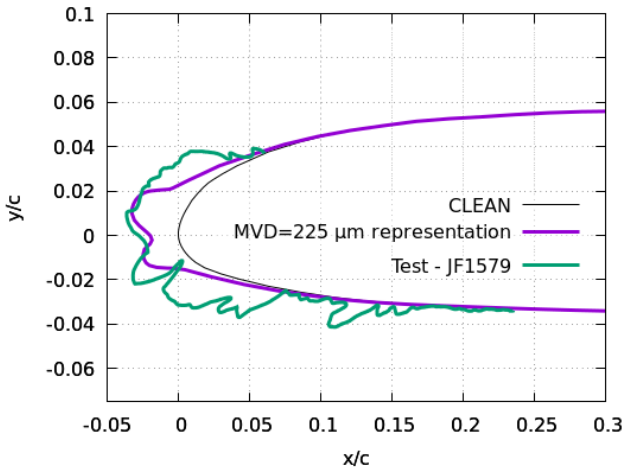

(d) MVD=225µm, U_∞=250kts, T_t=-10°C, LWC=0.38g/m^3

Figure 29. Commercial tail (chord = 36 inches): (a) (b) MVD ≈ 40 µm; (c) (d) MVD = 225 µm; (a) (c) U_∞ = 100 kts, T_t= -5°C; (b) (d) U_∞ = 250 kts, T_t = -10°C

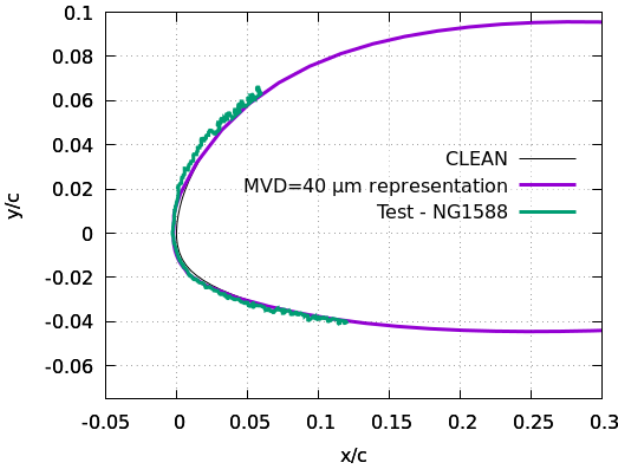

(a) MVD=40µm, U_∞=100kts, T_t=-5°C, LWC=0.32g/m^3

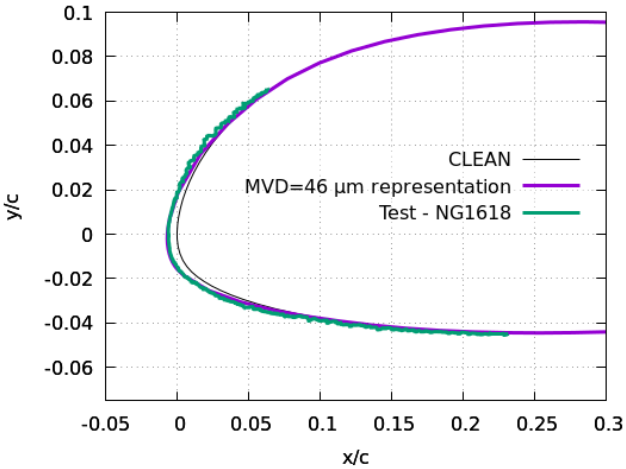

(b) MVD=46µm, U_∞=200 kts, T_t=-10°C, LWC=0.23g/m^3

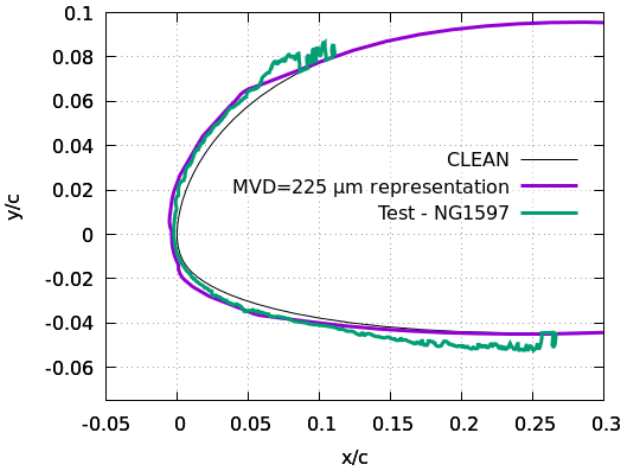

(c) MVD=225µm, U_∞=100kts, T_t=-5°C, LWC=1.39g/m^3

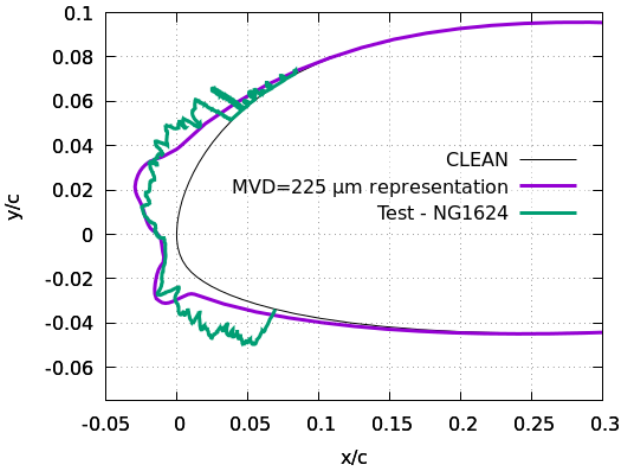

(d) MVD=225µm, U_∞=200kts, T_t=-10°C, LWC=0.80g/m^3

Figure 30. Business jet wing (chord = 61 inches): (a) (b) MVD ≈ 40 µm; (c) (d) MVD = 225 µm; (a) (c) U_∞ = 100 kts, T_t = -5°C; (b) (d) U_∞ = 200 kts, T_t = -10°C

SENSITIVITY TO SELECTED INPUT PARAMETERS

Some input parameters that may be under the control of the user may have a significant effect on the predicted ice shape. This is shown for time step and ice density. Included in this section are illustrations of sensitivity to MVD, although MVD is not under the control of the user in the same sense as time step or ice density, because when comparing to icing tunnel shapes, the MVD is specified

1. Sensitivity to time step:

   To examine the effect of user-defined time step on the final ice-shape predictions, one of the test cases of section 3, "FZRA, MVD > 40 μm distribution with LWC = 0.20 g/m^3," is repeated. The ice-accretion duration is increased to 45 minutes, and the angle of attack is set to 5^o. The rest of the input parameters are the same as those previously provided in section 3. Runs are conducted first using a single time step, then using multi-time step. Ice-shape results obtained with 10-bin and MVD representations of drop diameter distributions are shown in figures 31–33 using single, multi- (automated), and multi- (user set) time steps, respectively.

   There is a significant change in the results obtained with single-time step and that obtained with multi-time step (see figures 31–33).

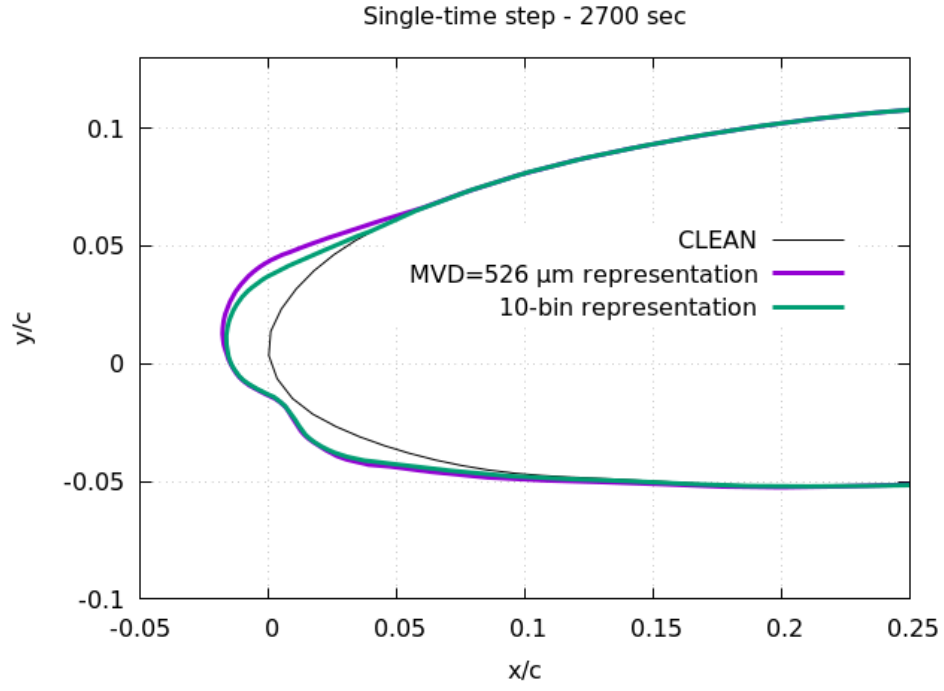

Figure 31. Single-time step, 45-min ice accretion

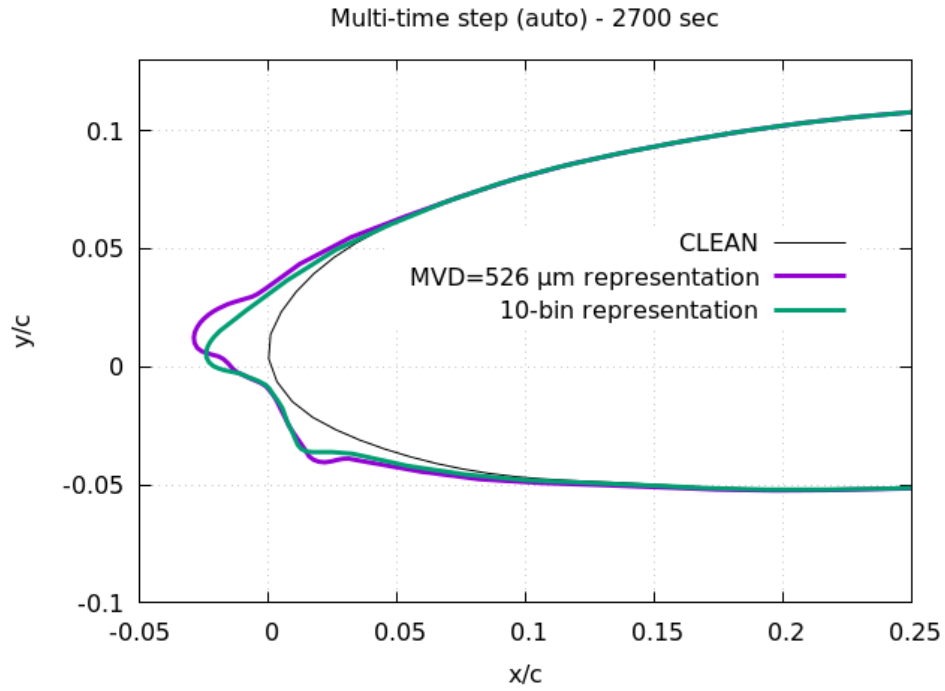

Figure 32. Multi-time step, 45-min ice accretion; time steps are automatically determined by LEWICE2D

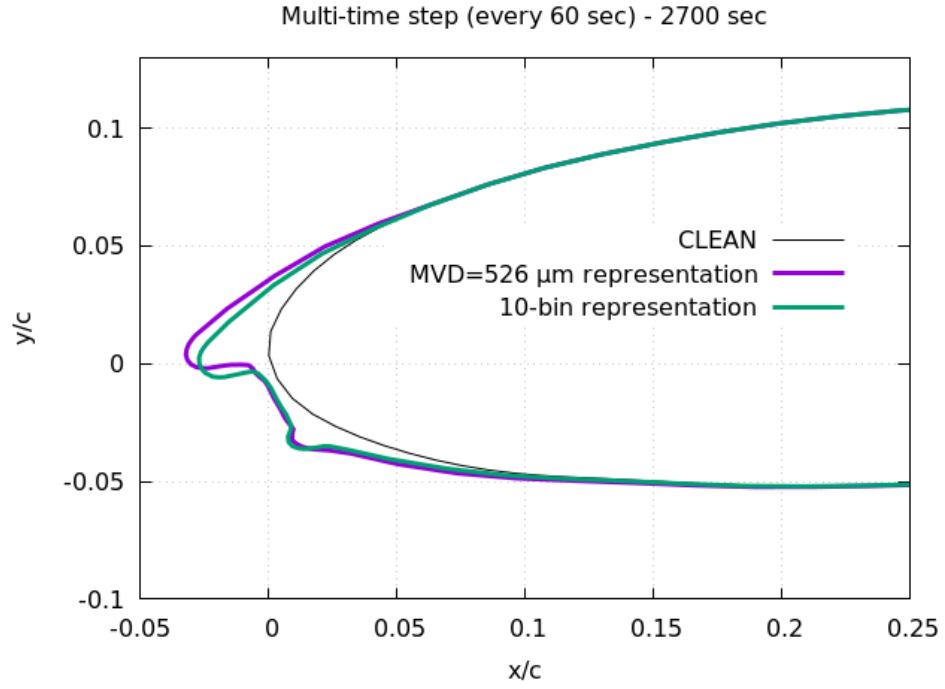

Figure 33. Multi-time step, 45-min ice accretion; time steps are 1 min apart

2. Sensitivity to ice density:

Two sets of simulations were conducted for dry- and wet-ice cases assuming mono-dispersed cloud distribution: first with MVD = 20 μm (SLD = 0), then with MVD = 320 μm (SLD = 1). In each set, three simulations were performed corresponding to a different constant ice density (ρ_{ice}) value of 300, 500, 917 kg/m^3. All simulations were started from input file of test case 7 given in the LEWICE2D manual. For dry-ice cases, T_∞=250 K, LWC = 0.3 g/m^3 were used; for wet ice cases, T_∞=266.85K, LWC=0.82 g/m^3 were used. The ice shape at the nose is caved in for SLD cases (see figures 34b and 35b). This must be due to "splashing" (i.e., losing/removing mass).

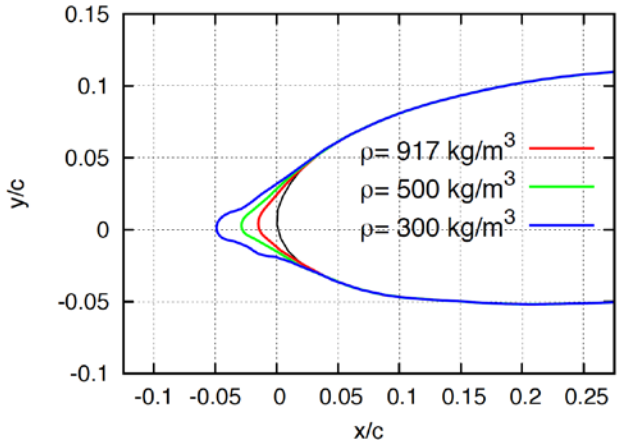

(a) MVD = 20 μm, SLD =0

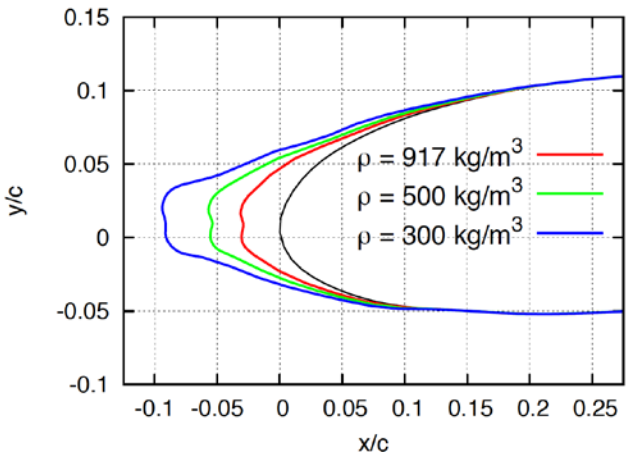

(b) MVD = 320 μm, SLD =1

Figure 34. Effect of ice density for dry-ice cases: monodispersed, T_∞=250 K, LWC = 0.3 g/m^3

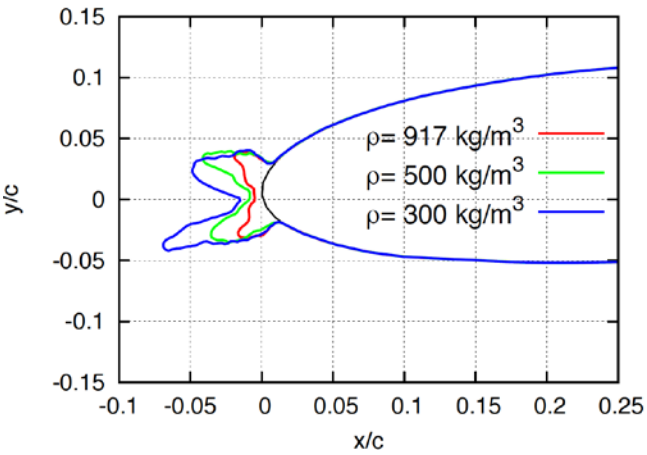

(a) MVD = 20 μm, SLD =0

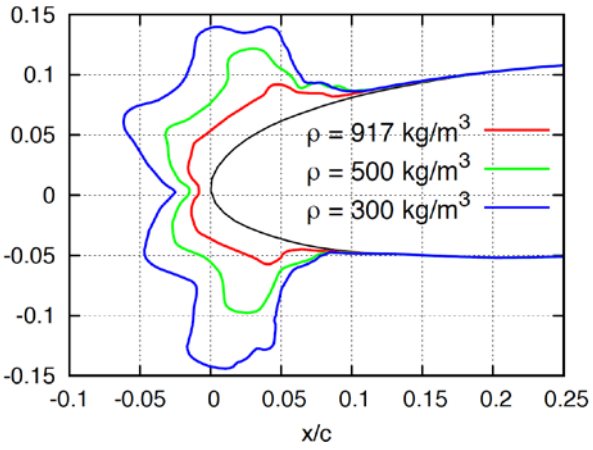

(b) MVD = 320 μm, SLD =1

Figure 35. Effect of ice density for wet-ice cases: monodispersed, T_∞=266.85 K, LWC=0.82 g/m^3

3. Sensitivity to mean volume diameter:

An early study of SLD icing conducted in the IRT is described in reference [4]. Conditions were set with different MVDs that should have given essentially the same ice shapes. However, they did not do so. Figures 3–4 from reference [4] are for dry-ice and wet-ice cases; they are reproduced below as figures 36a and 36b, respectively.

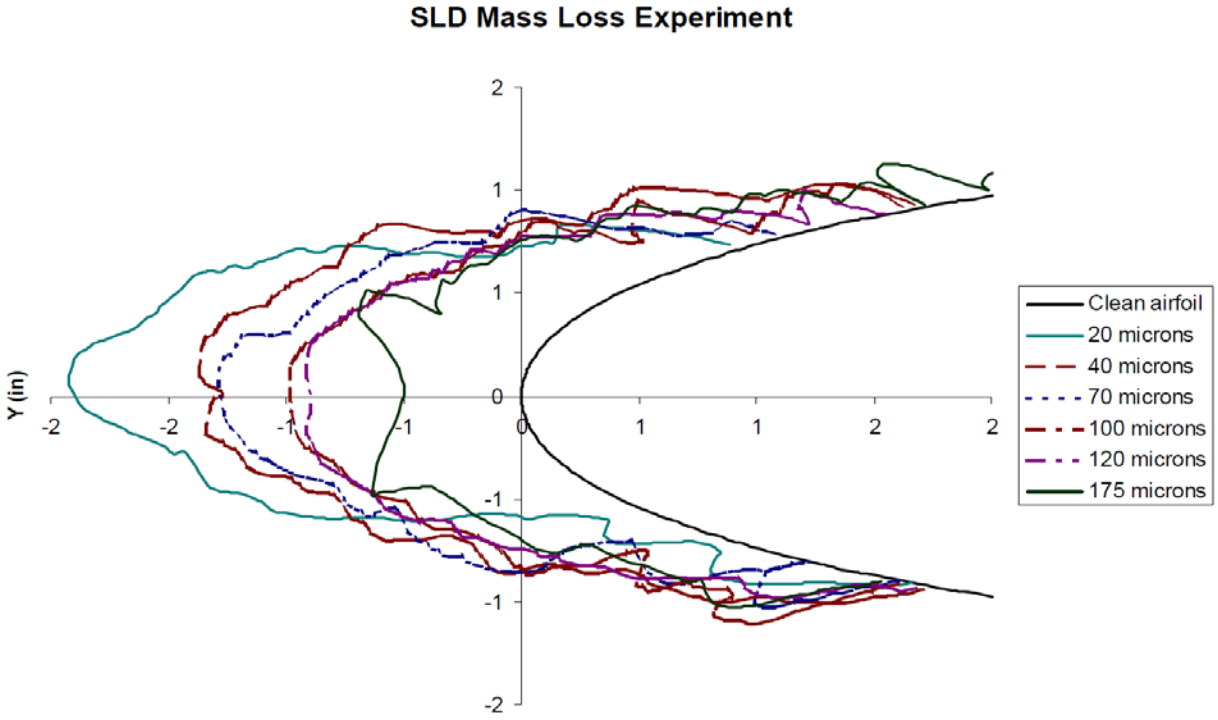

(a) Dry-ice cases

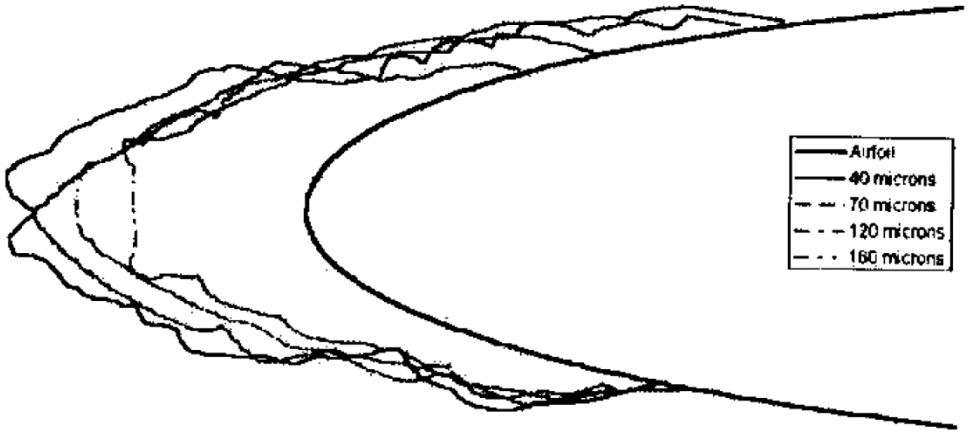

(b) Wet-ice cases

Figure 36. Ice-shape profiles from 21-inch chord NACA0012 airfoil [4]: (a) for dry-ice conditions tabulated in table 8, (b) for wet-ice conditions tabulated in table 9

Table 8. Test conditions for runs 1-18, 1-17, 1-1, 1-2, 1-5 and 1-4 [4]

Run No	MVD (μm)	LWC (g/m^3)	V (m/s)	T_{static} (K)	t (s)
1-18	20	1.03	104	248.94	714
1-17	40	1.02	77	251.14	588
1-1	70	0.91	51	252.35	804
1-2	100	0.98	51	252.45	618
1-5	120	1.03	52	252.31	548
1-4	160	1.50	52	252.41	300

Table 9. Test conditions for runs 1-22, 1-23, 1-24, 1-25 and 1-26 [4]

Run No	MVD (μm)	LWC (g/m^3)	V (m/s)	T_{static} (K)	t (s)
1-22	40	1.02	77	267.46	576
1-23	70	0.65	77	267.56	714
1-24	100	0.69	77	267.46	546
1-25	120	0.71	77	267.66	516
1-26	160	1.04	77	267.66	336

The same cases were run using LEWICE2D setting SLD = 1 for the cases with MVD $\geq$ 40 μm. The results are shown in figures 37a and 37b for dry- and wet-ice cases, respectively.

For dry-ice cases, the trend of decreasing ice-shape size with increasing MVD is similar to the experimental results. There are noticeable differences in ice shape as the MVD is increased. For wet-ice cases, the ice shapes are of roughly similar size and similar shape. The shapes predicted by LEWICE2D are also of roughly similar size and shape but are different from those observed experimentally. The total accreted mass is predicted higher for dry-ice cases, as shown in table 10.

Table 10. Comparison of measured [4] vs. predicted (LEWICE2D) mass

Run No	1-18	1-17	1-1	1-2	1-5	1-4	1-22	1-23	1-24	1-25	1-26
measured [4] (g)	736.4	698.1	566.3	502	487.9	420.8	695.7	605.7	546.7	548.4	545.4
predicted (LEWICE) (g)	1220	1094	1124	1047	1052	918	669	770	626	559	467

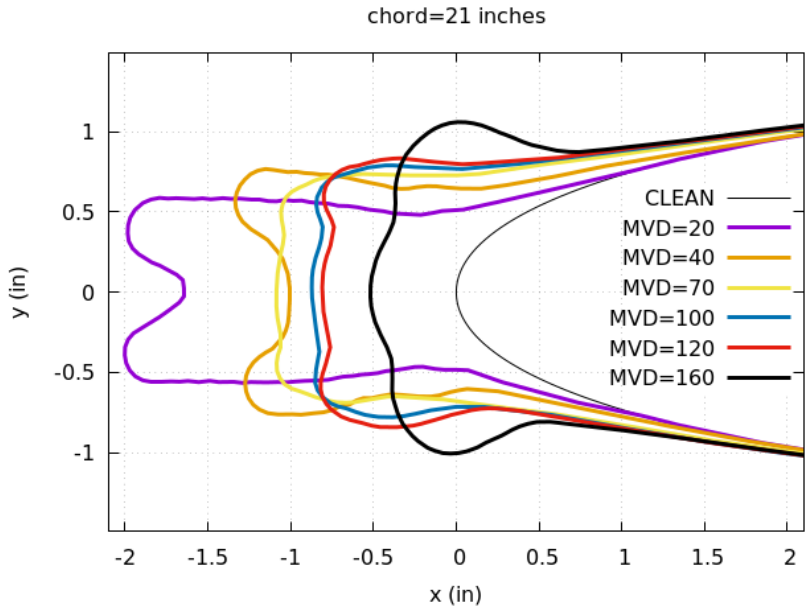

(a) Dry-ice cases

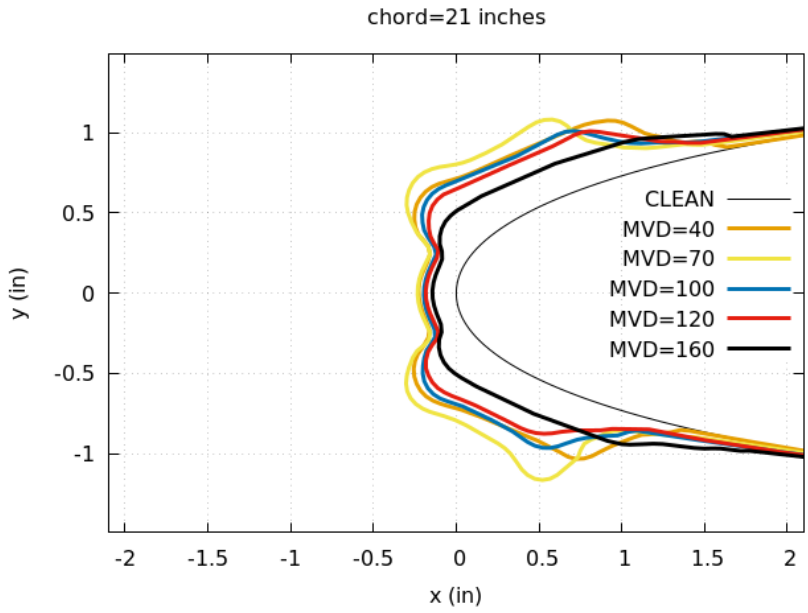

(b) Wet-ice cases

Figure 37. Ice-shape profiles from 21-inch chord NACA0012 airfoil obtained with LEWICE2D, version 3.2: (a) for dry-ice conditions tabulated in table 8, (b) for wet-ice conditions tabulated in table 9

The effect of chord size on ice shape is illustrated for several chord sizes in figures 38a–38d for increasing chord sizes.

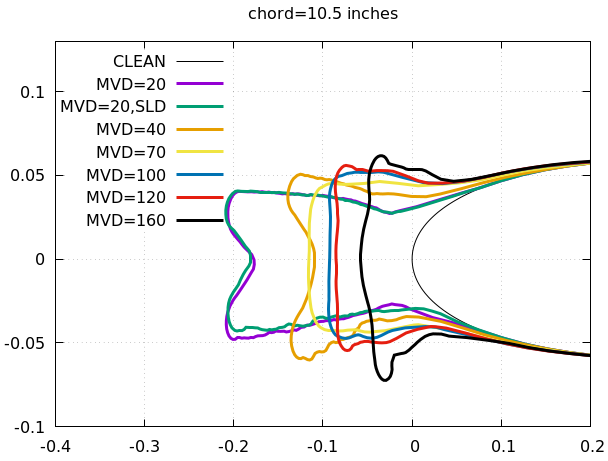

(a) Chord=10.5 inches

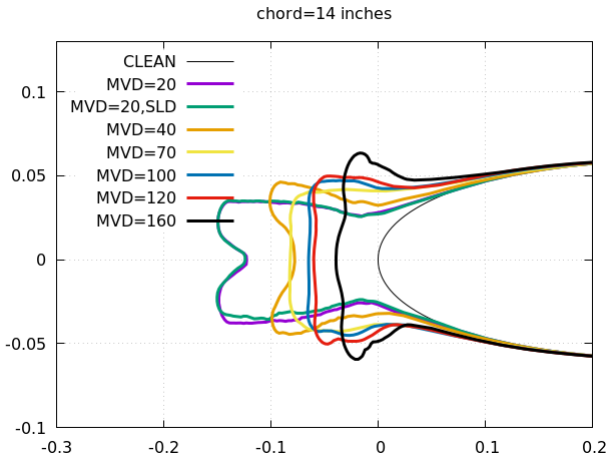

(b) Chord=14 inches

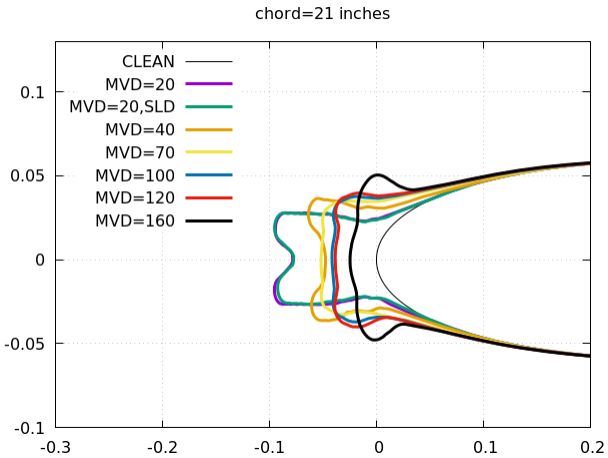

(c) Chord=21 inches

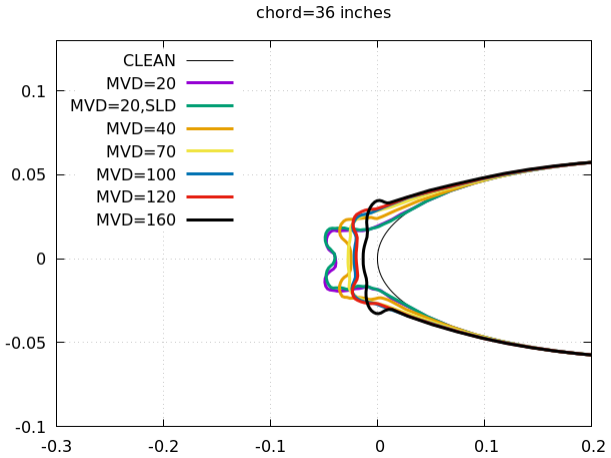

(d) Chord=36 inches

Figure 38. Effect of chord size on ice shape: (a) 10.5-inch chord, (b) 14-inch chord, (c) 21-inch chord, (d) 36-inch chord

CONCLUSIONS

Ice-shape comparisons have been conducted to show evaluation of the performance of 2D ice-accretion prediction computer codes for supercooled large drop (SLD) conditions.

The ice-shape prediction comparisons presented in this report addressed several issues: the fidelity of icing tunnel drop distributions to Title 14 Code of Federal Regulations Part 25, Appendix O distributions; the impact of using 10-bin versus MVD representations of the distributions; and the effect of liquid water content.

Ice-shape predictions were compared to experimental ice shapes from a database of SLD ice accretions developed through testing at NASA's Glenn Research Center's Icing Research Tunnel.

Also, sensitivity of ice shape to certain input parameters under the control of the users was briefly investigated.

The illustrations suggest that the shapes predicted by 2D ice-accretion computer codes may not be highly sensitive to differences in SLD drop distributions with 10-bin representations. Furthermore, they may not be highly sensitive to representations using MVD versus 10 bin, particularly for MVD>40.

Comparison to experimental ice shapes from the NASA Glenn IRT database showed similar trends, with some very good matching between predicted and experimental ice shapes. However, most all of the experimental shapes were very irregular, with large protuberances and feathers, and this was not captured by the ice-accretion code.

The ice-accretion code used for the illustrations showed significant sensitivity to some input parameters under the control of the user.

REFERENCES

1. NASA Report. (2008). User manual for the NASA Glenn Ice Accretion Code LEWICE Version 3.2.2. (NASA CR-2008-214255).

2. NASA Report. (2015). NASA Glenn Icing Research Tunnel: 2014 and 2015 Cloud Calibration Procedures and Results. (NASA/TM-2015-218758).

3. NASA Report. (2007). A database of supercooled large droplet ice accretions. (NASA/CR-2007-215020).

4. Potapczuk, M. (2003). Ice Mass Measurements: Implications for the ice accretion process, 41st Aerospace Sciences Meeting and Exhibit, AIAA 2003-387.

APPENDIX A–O TO PART 25: SUPERCOOLED LARGE DROP ICING CONDITIONS

This appendix consists of two parts. Part I defines this appendix as a description of supercooled large drop icing conditions in which the drop median volume diameter (MVD) is less than or greater than 40 μm, the maximum mean effective drop diameter (MED) of appendix C of this part continuous maximum (stratiform clouds) icing conditions. For this appendix, supercooled large drop icing conditions consist of freezing drizzle (FZDZ) and freezing rain (FZRA) occurring in or below stratiform clouds. Part II defines ice accretions used to show compliance with the airplane performance and handling qualities requirements of subpart B of this part.

PART I—METEOROLOGY

In this appendix, icing conditions are defined by the parameters of altitude, vertical and horizontal extent, temperature, liquid water content (LWC), and water mass distribution as a function of drop diameter distribution.

(a) FZDZ (conditions with spectra maximum drop diameters from 100–500 μm):

(1) Pressure altitude range: 0 to 22,000 ft MSL

(2) Maximum vertical extent: 12,000 ft

(3) Horizontal extent: Standard distance of 17.4 nautical miles

(4) Total LWC: See figure A-1

NOTE: LWC in grams per cubic meter (g/m3) based on horizontal extent standard distance of 17.4 nautical miles.

(5) Drop diameter distribution: see figure A-2

(6) Altitude and temperature envelope: see figure A-3

(b) FZRA (conditions with spectra maximum drop diameters greater than 500 μm):

(1) Pressure altitude range: 0 to 12,000 ft MSL

(2) Maximum vertical extent: 7000 ft

(3) Horizontal extent: Standard distance of 17.4 nautical miles

(4) Total LWC: See figure A-4

NOTE: LWC in grams per cubic meter (g/m3) based on horizontal extent standard distance of 17.4 nautical miles.

(5) Drop diameter distribution: see figure A-5.

(6) Altitude and temperature envelope: see figure A-6.

(c) Horizontal extent:

The LWC for FZDZ and FZRA conditions for horizontal extents other than the standard 17.4 nautical miles can be determined by the value of the LWC determined from figure A-1 or figure A-4, multiplied by the factor provided in figure A-7, which is defined by the following equation:

$$S = 1.266 - 0.213 \log_{10}(H)$$

where:

S = LWC Scale Factor (dimensionless) and

H = horizontal extent in nautical miles

PART II—AIRFRAME ICE ACCRETIONS FOR SHOWING COMPLIANCE WITH SUBPART B OF THIS PART

(a) *General*. The most critical ice accretion in terms of airplane performance and handling qualities for each flight phase must be used to show compliance with the applicable airplane performance and handling qualities requirements for icing conditions contained in subpart B of this part. Applicants must demonstrate that the full range of atmospheric icing conditions specified in part I of this appendix have been considered, including drop diameter distributions, LWC, and temperature appropriate to the flight conditions (for example, configuration, speed, angle of attack, and altitude).

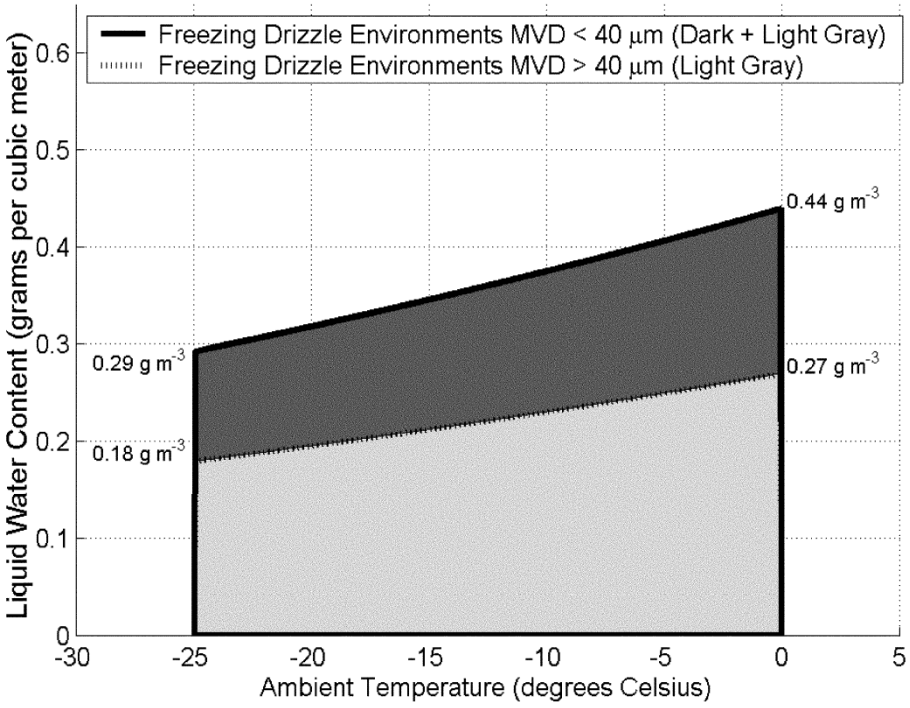

Figure A-1. Appendix O, FZDZ, LWC

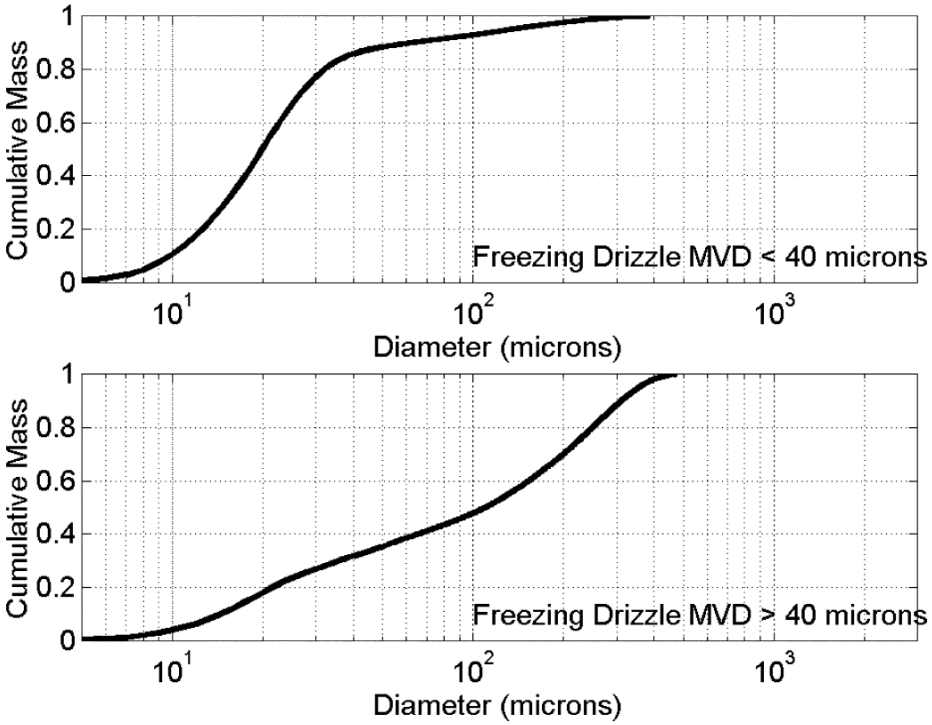

Figure A-2 Appendix O, FZDZ, drop diameter distribution

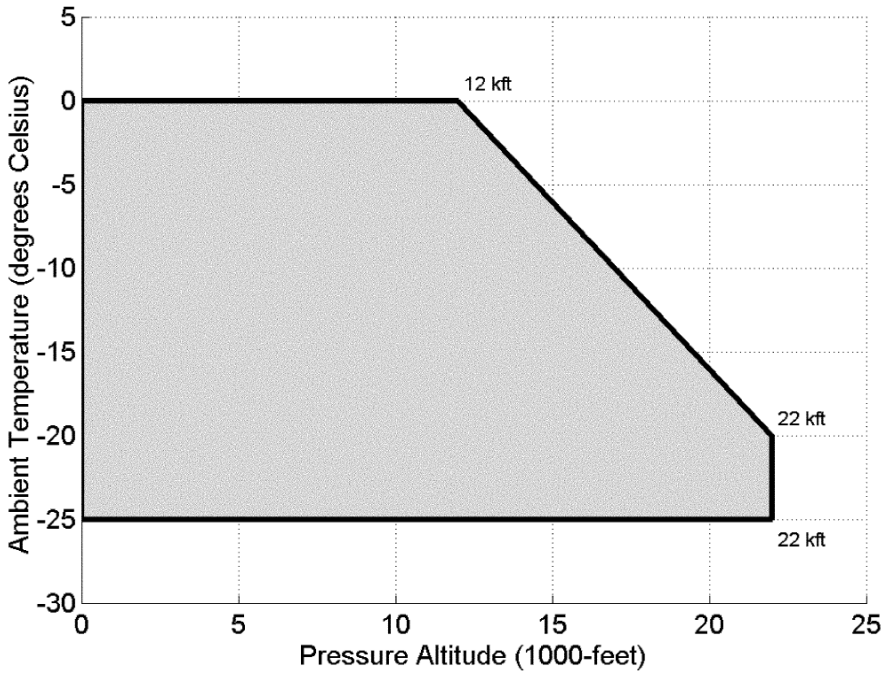

Figure A-3 Appendix O, FZDZ, temperature and altitude

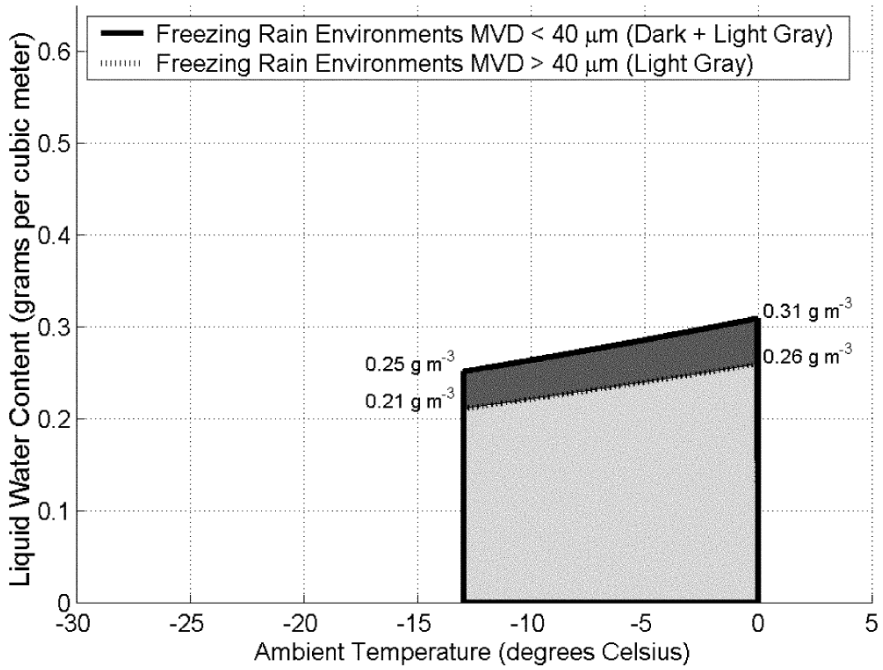

Figure A-4 Appendix O, FZRA, LWC

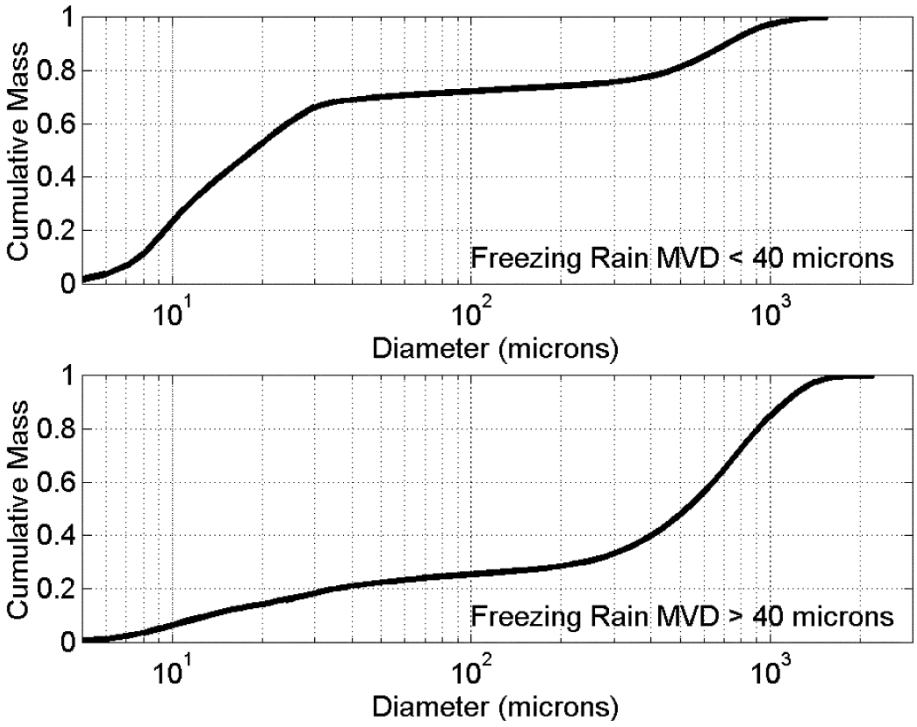

Figure A-5 Appendix O, FZRA, drop diameter distribution

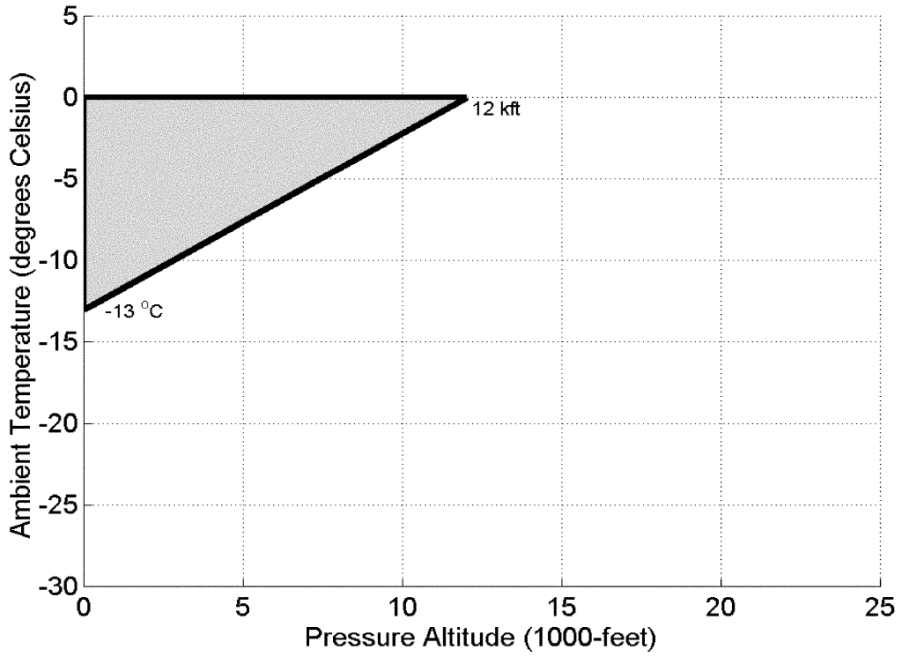

Figure A-6 Appendix O, FZRA, temperature and altitude

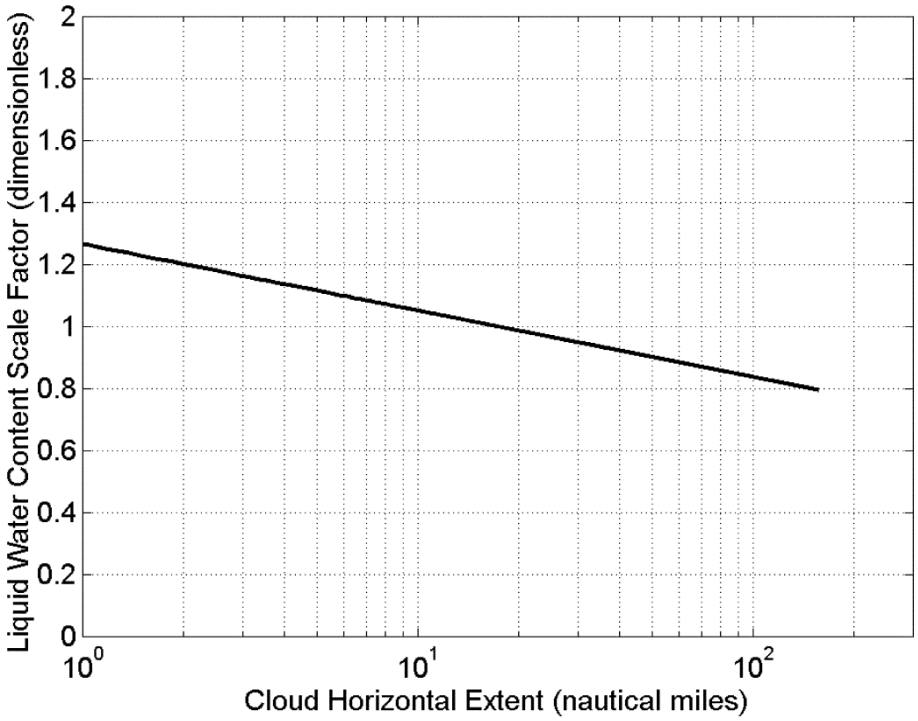

Figure A-7 Appendix O, horizontal extent, FZDZ and FZRA

(1) For an airplane certified in accordance with § 25.1420(a)(1), the ice accretions for each flight phase are defined in part II, paragraph (b) of this Appendix.

(2) For an airplane certified in accordance with § 25.1420(a)(2), the most critical ice accretion for each flight phase defined in part II, paragraphs (b) and (c) of this Appendix, must be used. For the ice accretions defined in part II, paragraph (c) of this Appendix, only the portion of part I of this Appendix in which the airplane is capable of operating safely must be considered.

(3) For an airplane certified in accordance with § 25.1420(a)(3), the ice accretions for each

flight phase are defined in part II, paragraph (c) of this Appendix.

(b) Ice accretions for airplanes certified in accordance with § 25.1420(a)(1) or (2).

(1) *En route ice* is the en route ice as defined by part II, paragraph (c)(3), of this Appendix, for an airplane certified in accordance with § 25.1420(a)(2), or defined by part II, paragraph (a)(3), of Appendix C of this part, for an airplane certified in accordance with § 25.1420(a)(1), plus:

(i) Pre-detection ice as defined by part II, paragraph (b)(5), of this Appendix; and

(ii) The ice accumulated during the transit of one cloud with a horizontal extent of 17.4 nautical miles in the most critical of the icing conditions defined in part I of this Appendix and one cloud with a horizontal extent of 17.4 nautical miles in the continuous maximum icing conditions defined in Appendix C of this part.

(2) *Holding ice* is the holding ice defined by part II, paragraph (c)(4), of this Appendix, for an airplane certified in accordance with § 25.1420(a)(2), or defined by part II, paragraph (a)(4), of Appendix C of this part, for an airplane certified in accordance with § 25.1420(a)(1), plus:

(i) Pre-detection ice as defined by part II, paragraph (b)(5), of this Appendix; and

(ii) The ice accumulated during the transit of one cloud with a 17.4 nautical miles horizontal extent in the most critical of the icing conditions defined in part I of this Appendix and one cloud with a horizontal extent of 17.4 nautical miles in the continuous maximum icing conditions defined in Appendix C of this part.

(iii) Except the total exposure to holding ice conditions does not need to exceed 45 minutes.

(3) *Approach ice* is the more critical of the holding ice defined by part II, paragraph (b)(2), of this Appendix, or the ice calculated in the applicable paragraphs (b)(3)(i) or (ii) of part II, of this Appendix:

(i) For an airplane certified in accordance with § 25.1420(a)(2), the ice accumulated during descent from the maximum vertical extent of the icing conditions defined in part I of this Appendix to 2,000 feet above the landing surface in the cruise configuration, plus transition to the approach configuration, plus:

(A) Pre-detection ice, as defined by part II, paragraph (b)(5), of this Appendix; and

(B) The ice accumulated during the transit at 2000 feet above the landing surface of one cloud with a horizontal extent of 17.4 nautical miles in the most critical of the icing conditions defined

in part I of this Appendix and one cloud with a horizontal extent of 17.4 nautical miles in the continuous maximum icing conditions defined in Appendix C of this part.

(ii) For an airplane certified in accordance with § 25.1420(a)(1), the ice accumulated during descent from the maximum vertical extent of the maximum continuous icing conditions defined in part I of Appendix C to 2000 feet above the landing surface in the cruise configuration, plus transition to the approach configuration, plus:

(A) Pre-detection ice, as defined by part II, paragraph (b)(5), of this Appendix; and

(B) The ice accumulated during the transit at 2000 feet above the landing surface of one cloud with a horizontal extent of 17.4 nautical miles in the most critical of the icing conditions defined in part I of this Appendix and one cloud with a horizontal extent of 17.4 nautical miles in the continuous maximum icing conditions defined in Appendix C of this part.

(4) *Landing ice* is the more critical of the holding ice as defined by part II, paragraph (b)(2), of this Appendix, or the ice calculated in the applicable paragraphs (b)(4)(i) or (ii) of part II of this Appendix:

(i) For an airplane certified in accordance with § 25.1420(a)(2), the ice accretion defined by part II, paragraph (c)(5)(i), of this Appendix, plus a descent from 2000 feet above the landing surface to a height of 200 feet above the landing surface with a transition to the landing configuration in the icing conditions defined in part I of this Appendix, plus:

(A) Pre-detection ice, as defined in part II, paragraph (b)(5), of this Appendix; and

(B) The ice accumulated during an exit maneuver, beginning with the minimum climb gradient required by § 25.119, from a height of 200 feet above the landing surface through one cloud with a horizontal extent of 17.4 nautical miles in the most critical of the icing conditions defined in part I of this Appendix and one cloud with a horizontal extent of 17.4 nautical miles in the continuous maximum icing conditions defined in Appendix C of this part.

(ii) For an airplane certified in accordance with § 25.1420(a)(1), the ice accumulated in the maximum continuous icing conditions defined in Appendix C of this part, during a descent from the maximum vertical extent of the icing conditions defined in Appendix C of this part, to 2000 feet above the landing surface in the cruise configuration, plus transition to the approach configuration and flying for 15 minutes at 2000 feet above the landing surface, plus a descent from 2000 feet above the landing surface to a height of 200 feet above the landing surface with a transition to the landing configuration, plus:

(A) Pre-detection ice, as described by part II, paragraph (b)(5), of this Appendix; and

(B) The ice accumulated during an exit maneuver, beginning with the minimum climb gradient required by § 25.119, from a height of 200 feet above the landing surface through one cloud with a horizontal extent of 17.4 nautical miles in the most critical of the icing conditions defined in part I of this Appendix and one cloud with a horizontal extent of 17.4 nautical miles in the continuous maximum icing conditions defined in Appendix C of this part.

(5) *Pre-detection ice* is the ice accretion before detection of flight conditions in this Appendix that require exiting per § 25.1420(a)(1) and (2). It is the pre-existing ice accretion that may exist from operating in icing conditions in which the airplane is approved to operate prior to encountering the icing conditions requiring an exit, plus the ice accumulated during the time needed to detect the icing conditions, followed by 2 minutes of further ice accumulation to take into account the time for the flight crew to take action to exit the icing conditions, including coordination with air traffic control.

(i) For an airplane certified in accordance with § 25.1420(a)(1), the pre-existing ice accretion must be based on the icing conditions defined in Appendix C of this part.

(ii) For an airplane certified in accordance with § 25.1420(a)(2), the pre-existing ice accretion must be based on the more critical of the icing conditions defined in Appendix C of this part, or the icing conditions defined in part I of this Appendix in which the airplane is capable of safely operating.

(c) *Ice accretions for airplanes certified in accordance with §§ 25.1420(a)(2) or (3).* For an airplane certified in accordance with § 25.1420(a)(2), only the portion of the icing conditions of part I of this Appendix in which the airplane is capable of operating safely must be considered.

(1) *Takeoff ice* is the most critical ice accretion on unprotected surfaces, and any ice accretion on the protected surfaces, occurring between the end of the takeoff distance and 400 feet above the takeoff surface, assuming accretion starts at the end of the takeoff distance in the icing conditions defined in part I of this Appendix.

(2) *Final takeoff ice* is the most critical ice accretion on unprotected surfaces, and any ice accretion on the protected surfaces appropriate to normal ice protection system operation, between 400 feet and either 1500 feet above the takeoff surface, or the height at which the transition from the takeoff to the en route configuration is completed and VFTO is reached, whichever is higher. Ice accretion is assumed to start at the end of the takeoff distance in the icing conditions defined in part I of this Appendix.

(3) *En route ice* is the most critical ice accretion on the unprotected surfaces, and any ice accretion on the protected surfaces appropriate to normal ice protection system operation, during the en route flight phase in the icing conditions defined in part I of this Appendix.

(4) *Holding ice* is the most critical ice accretion on the unprotected surfaces, and any ice accretion on the protected surfaces appropriate to normal ice protection system operation, resulting from 45 minutes of flight within a cloud with a 17.4 nautical miles horizontal extent in the icing conditions defined in part I of this Appendix, during the holding phase of flight.

(5) *Approach ice* is the ice accretion on the unprotected surfaces, and any ice accretion on the protected surfaces appropriate to normal ice protection system operation, resulting from the more critical of the:

(i) Ice accumulated in the icing conditions defined in part I of this Appendix during a descent from the maximum vertical extent of the icing conditions defined in part I of this Appendix, to

2000 feet above the landing surface in the cruise configuration, plus transition to the approach configuration and flying for 15 minutes at 2000 feet above the landing surface; or

(ii) Holding ice as defined by part II, paragraph (c)(4), of this Appendix.

(6) *Landing ice* is the ice accretion on the unprotected surfaces, and any ice accretion on the protected surfaces appropriate to normal ice protection system operation, resulting from the more critical of the:

(i) Ice accretion defined by part II, paragraph (c)(5)(i), of this Appendix, plus ice accumulated in the icing conditions defined in part I of this Appendix during a descent from 2000 feet above the landing surface to a height of 200 feet above the landing surface with a transition to the landing configuration, followed by a go-around at the minimum climb gradient required by § 25.119, from a height of 200 feet above the landing surface to 2000 feet above the landing surface, flying for 15 minutes at 2000 feet above the landing surface in the approach configuration, and a descent to the landing surface (touchdown) in the landing configuration; or

(ii) Holding ice as defined by part II, paragraph (c)(4), of this Appendix.

(7) For both unprotected and protected parts, the ice accretion for the takeoff phase must be determined for the icing conditions defined in part I of this Appendix, using the following assumptions:

(i) The airfoils, control surfaces, and, if applicable, propellers are free from frost, snow, or ice at the start of takeoff;

(ii) The ice accretion starts at the end of the takeoff distance;

(iii) The critical ratio of thrust/power-to-weight;

(iv) Failure of the critical engine occurs at VEF; and

(v) Crew activation of the ice protection system is in accordance with a normal operating procedure provided in the airplane flight manual, except that after beginning the takeoff roll, it must be assumed that the crew takes no action to activate the ice protection system until the airplane is at least 400 feet above the takeoff surface.

(d) The ice accretion before the ice protection system has been activated and is performing its intended function is the critical ice accretion formed on the unprotected and normally protected surfaces before activation and effective operation of the ice protection system in the icing conditions defined in part I of this Appendix. This ice accretion only applies in showing compliance to §§ 25.143(j) and 25.207(h).

(e) To reduce the number of ice accretions to be considered when demonstrating compliance with the requirements of § 25.21(g), any of the ice accretions defined in this Appendix may be used for any other flight phase if it is shown to be at least as critical as the specific ice accretion defined for that flight phase. Configuration differences and their effects on ice accretions must be taken into account.

(f) The ice accretion that has the most adverse effect on handling qualities may be used for airplane performance tests provided any difference in performance is conservatively taken into account.

[Amdt. 25–140, 79 FR 65528, Nov. 4, 2014]